UNIVERSIDAD DE INVESTIGACIÓN DE TECNOLOGÍA EXPERIMENTAL YACHAY

Escuela de Ciencias Físicas y Nanotecnología

TÍTULO: Study of the Scalar Power Spectrum for the chaotic inflationary model with a step

Trabajo de integración curricular presentado como requisito para la obtención del título de Físico

Autor:

Calvache Trávez Lenin

Tutor:

PhD. Rojas Cely Clara

Urcuquí, Julio 2022

SECRETARÍA GENERAL
(Vicerrectorado Académico/Cancillería)
ESCUELA DE CIENCIAS FÍSICAS Y NANOTECNOLOGÍA
CARRERA DE FÍSICA
ACTA DE DEFENSA No. UITEY-PHY-2022-00010-AD

A los 27 días del mes de junio de 2022, a las 10:00 horas, de manera virtual mediante videoconferencia, y ante el Tribunal Calificador, integrado por los docentes:

Presidente Tribunal de Defensa	Mgs. ANDRADE ACOSTA, DAVID MARCOS
Miembro No Tutor	Dr. COSENZA MICELI, MARIO GIUSEPPE , Ph.D.
Tutor	Dra. ROJAS CELY CLARA INES , Ph.D.

El(la) señor(ita) estudiante **CALVACHE TRAVEZ, LENIN WLADIMIR**, con cédula de identidad No. **1727284158**, de la **ESCUELA DE CIENCIAS FÍSICAS Y NANOTECNOLOGÍA**, de la Carrera de **FÍSICA**, aprobada por el Consejo de Educación Superior (CES), mediante Resolución **RPC-SO-39-No.456-2014**, realiza a través de videoconferencia, la sustentación de su trabajo de titulación denominado: **STUDY OF THE SCALAR POWER SPECTRUM FOR THE CHAOTIC INFLATIONARY MODEL WITH A STEP**, previa a la obtención del título de **FÍSICO/A**.

El citado trabajo de titulación, fue debidamente aprobado por el(los) docente(s):

Tutor	Dra. ROJAS CELY CLARA INES , Ph.D.

Y recibió las observaciones de los otros miembros del Tribunal Calificador, las mismas que han sido incorporadas por el(la) estudiante.

Previamente cumplidos los requisitos legales y reglamentarios, el trabajo de titulación fue sustentado por el(la) estudiante y examinado por los miembros del Tribunal Calificador. Escuchada la sustentación del trabajo de titulación a través de videoconferencia, que integró la exposición de el(la) estudiante sobre el contenido de la misma y las preguntas formuladas por los miembros del Tribunal, se califica la sustentación del trabajo de titulación con las siguientes calificaciones:

Tipo	Docente	Calificación
Presidente Tribunal De Defensa	Mgs. ANDRADE ACOSTA, DAVID MARCOS	9,5
Miembro Tribunal De Defensa	Dr. COSENZA MICELI, MARIO GIUSEPPE , Ph.D.	10,0
Tutor	Dra. ROJAS CELY CLARA INES , Ph.D.	10,0

Lo que da un promedio de: **9.8 (Nueve punto Ocho)**, sobre 10 (diez), equivalente a: **APROBADO**

Para constancia de lo actuado, firman los miembros del Tribunal Calificador, el/la estudiante y el/la secretario ad-hoc.

CALVACHE TRAVEZ, LENIN WLADIMIR
Estudiante

Firmado electrónicamente por:
LENIN WLADIMIR CALVACHE TRAVEZ

Mgs. ANDRADE ACOSTA, DAVID MARCOS
Presidente Tribunal de Defensa

Firmado electrónicamente por:
DAVID MARCOS ANDRADE ACOSTA

Dra. ROJAS CELY CLARA INES , Ph.D.
Tutor

CLARA INES ROJAS CELY
Digitally signed by CLARA INES ROJAS CELY
Date: 2022.06.28 14:02:49 -05'00'

Dr. COSENZA MICELI, MARIO GIUSEPPE , Ph.D.
Miembro No Tutor

Firmado electrónicamente por:
MARIO GIUSEPPE COSENZA MICELI

DE LA CRUZ ZAPATA, TANIA DANIELA
Secretario Ad-hoc

AUTORÍA

Yo, **LENIN WLADMIR CALVACHE TRAVEZ**, con cédula de identidad 1727284158, declaro que las ideas, juicios, valoraciones, interpretaciones, consultas bibliográficas, definiciones y conceptualizaciones expuestas en el presente trabajo; así cómo, los procedimientos y herramientas utilizadas en la investigación, son de absoluta responsabilidad de el/la autora (a) del trabajo de integración curricular. Así mismo, me acojo a los reglamentos internos de la Universidad de Investigación de Tecnología Experimental Yachay.

Urcuquí, Julio 2022.

Firmado electrónicamente por:
LENIN WLADIMIR CALVACHE TRAVEZ

_____

Lenin Wladimir Calvache Trávez

CI: 1727284158

AUTORIZACIÓN DE PUBLICACIÓN

Yo, **LENIN WLADIMIR CALVACHE TRAVEZ,** con cédula de identidad 1727284158, cedo a la Universidad de Investigación de Tecnología Experimental Yachay, los derechos de publicación de la presente obra, sin que deba haber un reconocimiento económico por este concepto. Declaro además que el texto del presente trabajo de titulación no podrá ser cedido a ninguna empresa editorial para su publicación u otros fines, sin contar previamente con la autorización escrita de la Universidad.

Asimismo, autorizo a la Universidad que realice la digitalización y publicación de este trabajo de integración curricular en el repositorio virtual, de conformidad a lo dispuesto en el Art. 144 de la Ley Orgánica de Educación Superior

Urcuquí, Julio 2022.

Firmado electrónicamente por:
LENIN WLADIMIR CALVACHE TRAVEZ

_____

Lenin Wladimir Calvache Trávez

CI: 1727284158

Acknowledgements

First, I want to express my gratitude to my mom, Lidia, for her support, trust and love during all the time I was studying. I also, want to thank my father, Eduardo, and my sisters, Martha, Alexandra and Karla for their advice and support.

I would like to express my gratitude to my advisor, Ph. D. Clara Rojas, for all the time and knowledge she shared with me and for her patience. Thanks for believe in me and give me the opportunity and the guide to accomplish this work.

I also want to thank my second family in Yachay, Andres, Diego, Milton, Joshua, Jose, Rony, Daniel and Pol for all the time we spent together. Additionally, I want to thank all the professors I met in Yachay for all the knowledge they shared with me.

Lenin Wladimir Calvache Trávez

Resumen

La radiación de Fondo Cósmico de Microondas (CMB, por sus siglas en inglés) es la evidencia más notable que respalda la cosmología del Big Bang y ha sido una herramienta fundamental para comprender el Universo primitivo. La mayoría de la información codificada en el CMB se encuentra en su campo de temperatura. Su espectro de energía tiene una forma de cuerpo negro casi perfecta, sin embargo, exhibe anisotropías al nivel de $\delta T/T \sim 10^{-5}$. La cosmología de la inflación nos ayuda a explicar características de esta radiación que la teoría del Big Bang no puede explicar. El propósito de este trabajo es utilizar un potencial caótico con una característica para reproducir y estudiar el espectro de potencia angular del CMB. Para la obtención del espectro se utilizó el Código de Anisotropías en el Fondo de Microondas (CAMB, por sus siglas en inglés). El potencial que utilizamos para este estudio tiene tres parámetros libres (c, d and φ_{step}) y encontramos un conjunto de valores para estos parámetros que mejor reproduce el espectro de potencia angular con respecto a los datos de la colaboración Planck (con un error relativo menor a 0.09). La posición y amplitud de los picos encontrados con nuestro potencial son similares a los reportados por la colaboración Planck, de hecho, algunos valores están dentro del rango de error. Además, usando CAMB encontramos los valores de algunos parámetros cosmológicos; edad del universo, Ω_m, Ω_b, Ω_Λ and Ω_K. También calculamos el índice espectral escalar, $n_s = 0.966942$, y sus términos asociados.

Palabras Clave:

Fondo Cósmico de Microondas, parámetros cosmológicos, anisotropías, oscilaciones acústicas, escalas angulares.

Abstract

Cosmic Microwave Background (CMB) radiation is the most remarkable evidence that support the Big Bang cosmology and has been a fundamental tool to understand the early Universe. The vast majority of information encoded in the CMB lies in its temperature field. Its energy spectrum has a nearly perfect black body shape, however, it exhibits anisotropies at the level of $\delta T/T \sim 10^{-5}$. Inflation cosmology helps us to explain features of this radiation that the Big Bang theory cannot. The purpose of this work is to use a chaotic potential with a step to reproduce and study the angular power spectrum of the CMB. In order to obtain the spectrum, the Code for Anisotropies in the Microwave Background (CAMB) was used. The potential we used for this study has three free parameters (c, d and φ_{step}) and we found a set of values for these parameters which best reproduces the angular power spectrum with respect to the data of Planck Collaboration (with a relative error < 0.09). The position and amplitude of the peaks found with our potential are similar to the reported by Planck collaboration, in fact, some values are inside the range of error. Additionally, using CAMB we found the values of a few cosmological parameters; age of the Universe, Ω_m, Ω_b, Ω_Λ and Ω_K. Besides, we computed the scalar spectral index, $n_s = 0.966942$, and its running terms.

Keywords:

Cosmic Microwave Background, cosmological parameters, anisotropies, acoustic oscillations, angular scales.

Contents

List of Figures

List of Tables

Chapter 1

Introduction

The study of the Universe on its largest scales was once the least precise in all astrophysics. The vast distances made accurate measurements near impossible. However, as our telescopes and our techniques improved over the last few decades, we now live in an era of precision cosmology. In fact, we know to stunning detail the properties that govern the birth, evolution and the end of our universe. One of the most remarkable observations is the Cosmic Microwave Background (CMB) radiation, this radiation is the remnants of an epoch known as recombination where the hot dense universe became transparent for the first time. In 1948, Alpher and Herman predicted that the temperature of CMB had to be 5 K[7]. Later, in 1965 Penzias and Wilson measured by "accident" the CMB, when they were looking at the sky they measured a background noise temperature of about 3.5 K[8].

CMB provides information from 370,000 years after the very birth of the universe and from its discovery the precision in its measurement has increased dramatically. In fact, Far-InfraRed Absolute Spectrophotometer (FIRAS) experiment has measured the temperature of the CMB to an extraordinary precision of 2.72548 ± 0.00057 K[4,9]. A surprising feature of the CMB was its almost perfect black body distribution which is interpreted as evidence of the Big Bang and resulting in a homogeneous and isotropic universe.

After the discovery of CMB, the next goal was to look for spectral distorsions in the black body shape of the spectrum and anisotropies in the CMB. The reason for this was that the CMB should have evidence of the initial fluctuations resulting by gravitational stability and these fluctuations were assumed to be the origin of the structure of the present universe[10]. Theoretical studies of these anisotropies were performed such as the prediction of the physical processes that could generate them (e.g. gravitational redshift and diffusion damping)[11,12], the evolution of the density perturbations[13] and the consequences of the thermal history and structure formation of the universe on the CMB[14]. Despite the studies began soon after the discovery of Penzias and Wilson, the observations of those days could not corroborate these studies due to technological limitations to perform experiments that could measure the anisotropies.

The dipole anisotropy was the first measurement of the anisotropies on the CMB[15,16], but this anisotropy is the result of the Doppler effect due to the peculiar motion of the solar system relative to the rest frame of the CMB. In 1989, Cosmic Background Explorer (COBE) satellite was launched and it measured temperature anisotropies in

the CMB [17] on the level of $\delta T/T \sim 10^{-5}$. COBE's discovery led to theoretical work that helps to understand the inherent features of the CMB and this revealed the need of improving the precision of the measurements of CMB. As a result, Wilkinson Microwave Anisotropy Probe (WMAP) and Plack missions were carried out by NASA and ESA, respectively. In 2001 MAP satellite, later called WMAP, was launched and reported the first results in 2003 [18,19]. It took nine years of data on 5 frequencies and mapped the full sky CMB anisotropy, the final results were reported in 2013 [20]. In 2009 Planck satellite was launched and it was scanning the sky for four years. It collected data in nine frequency bands from 30 to 857 GHz, this allows to produce deep and high resolution maps of all sky. These results along with calculation of cosmological parameters were reported in 2018 [21–23].

1.1 Problem Statement

The Hot Big Bang Theory is the accepted theory that explains the evolution of our Universe. However, this theory presents some problems that can not be explained such as the flatness problem, the horizon problem and others [24–26]. In order to solve these problems a new theory was born, the inflationary theory. The simplest inflationary scenarios is based on a scalar field ϕ rolling down a smooth potential $V(\phi)$. There exist several models, however, thanks to the improvement in the measurements of the CMB it is possible to assess these models and find the ones that fits better the data reported by Planck Collaboration [23].

1.2 General and Specific Objectives

General Objective:

Reproduce and study the angular power spectrum of the CMB with the chaotic inflationary model with a step into the slow-roll approximation. For this purpose the Code for Anisotropies in the Microwave Background (CAMB) will be used.

Specific Objectives:

1. Find the best parameters of the potential that allows to reproduce with more accuracy the angular power spectrum of the CMB.

2. Study in detail the different regions of the angular power spectrum.

3. Assess the relation of the angular power spectrum with the value of cosmological parameters.

Throughout this work natural units will be used ($c = \hbar = 1$) and reduced Planck mass $M_{pl} = 1$.

Chapter 2

Methodology

2.1 The Hot Big Bang Theory

Modern cosmology is based on the Cosmological Principle, which tells us that the Universe is homogeneous and isotropic at large scales[27]. It also is the basis of the Big Bang Cosmology that explains the development of the universe from a much hotter and denser earlier universe[5]. This model of cosmology is supported by a number of observational evidence among them are the Hubble's law that explains the expansion of the universe, the existence of the Cosmic Microwave Background (CMB), and the Nucleosynthesis that explains abundances of the light elements. Furthermore, there is a theoretical foundation to explain the evolution of the universe; General Relativity (GR) developed by Albert Einstein.

2.1.1 Theoretical bases

In a curved spacetime, the metric gives the physical distance between two infinitesimally close points defined in some arbitrary coordinate system[5]. From the premise that the Universe is homogeneous and isotropic at large scales, the most general metric that satisfies this condition is the Friedmann–Robertson–Walker (FRW) metric

$$ds^2 = -dt^2 + a(t)\left[\frac{dr^2}{1 - kr^2} + r^2(d\theta^2 + \sin^2\theta d\phi^2)\right],\tag{2.1}$$

where t is time, r, θ and ϕ are comoving spatial coordinates. The scale factor, $a(t)$, is a time dependent quantity that characterizes the expansion of the universe, and k is a parameter that measures the curvature of space. The parameter k can take the values 1, 0 and -1 for positive, zero, and negative curvature respectively.

The dynamics evolution of the universe is contained in the Einstein equations. The set of equations can be summarized as the tensor equality

$$G_{\mu\nu} + \Lambda g_{\mu\nu} = 8\pi G T_{\mu\nu},\tag{2.2}$$

where G is the gravitational constant, Λ is the cosmological constant and $G_{\mu\nu}$ is the Einstein tensor defined by

$$G_{\mu\nu} \equiv R_{\mu\nu} - \frac{1}{2}g_{\mu\nu}R, \tag{2.3}$$

here $R_{\mu\nu}$ is the *Ricci tensor* and R is the Ricci scalar ($R \equiv g^{\mu\nu}R_{\mu\nu}$).

Applying the field equations of GR to the FRW metric we obtain the Friedmann equations[28]

$$H^2 = \left(\frac{\dot{a}}{a}\right)^2 = \frac{8\pi G\rho}{3} - \frac{k}{a^2} + \frac{\Lambda}{3}, \tag{2.4}$$

$$\frac{\ddot{a}}{a} = -\frac{4\pi G}{3}(\rho + 3p) + \frac{\Lambda}{3}, \tag{2.5}$$

where $H = \dot{a}/a$ is the Hubble parameter, ρ and p are the total energy density (matter, radiation and dark energy) and the total pressure of the Universe, respectively. Eq. (2.5) is also known as the acceleration equation.

The evolution of the energy density is ruled by the equation-of-state parameter, $w_i \equiv p_i/\rho_i$. The subindices i stands for the constituents of the universe: matter (m), radiation (r) and vacuum energy (vac). For a constant w_i

$$w_i = \frac{p_i}{\rho_i} = constant, \tag{2.6}$$

The equation-of-state parameter for each component is

$$\begin{aligned} w_m &= 0, & \text{matter,} \\ w_r &= 1/3, & \text{radiation,} \\ w_{vac} &= -1, & \text{vacuum energy.} \end{aligned} \tag{2.7}$$

The critical energy density ρ_c is given by

$$\rho_c = \frac{3H^2}{8\pi G}, \tag{2.8}$$

and its present value is $\rho_c = 8.10 \times 10^{-47}h^2$ GeV. It allows to normalize the cosmic energy densities as

$$\Omega_i = \frac{\rho_i(t_0)}{\rho_c}, \tag{2.9}$$

this is the density parameter. $\Omega_0 > 1$ results in a positively curved Universe, while $\Omega_0 < 1$ gives a negatively curved Universe. The information from the CMB suggests that the Universe is nearly spatially flat ($\Omega = 1$).

The evolution of the energy density with respect to the scale factor is given by

$$\rho \propto a^{-3(1+w)}, \tag{2.10}$$

so, for the different constituents we have

$$\rho \propto a^{-4}, \qquad \text{radiation,}$$
$$\rho \propto a^{-3}, \qquad \text{matter,} \qquad\qquad\qquad\qquad (2.11)$$
$$\rho \propto a^{0}, \qquad \text{cosmological constant.}$$

The evolution of the scale factor depends on the dominant energy form, given by

$$a(t) \propto t^{2/3(1+w)}, \qquad\qquad\qquad\qquad (2.12)$$

and the Universe has gone through a radiation dominated era, $a(t) \propto t^{1/2}$, a matter dominated era, $a(t) \propto t^{2/3}$, and a dark energy dominated era, $a(t) \propto \exp(Ht)$.

2.2 Obsevational evidence of Big Bang

2.2.1 Hubble's law

Nowadays it is well known and we have solid evidence that the universe is expanding, however, around 100 years ago the prevailing picture was a static universe. The first hints of an evolving universe were given by Alexander Friedmann and Georges Lemaitre. In 1922 Friedmann found that Einstein's equations allow a dynamical universe[29] and in 1927 Lemaitre derived a nonstatic solution to Einstein's equations and based on observational evidence he suggested that the universe is expanding[30]. In 1929, conclusive evidence was provided by Edwin Hubble, he found a correlation between distance and recession velocity of galaxies[31]. This changed our understanding of the universe. This relation is the known as the Hubble Law (also known as Hubble-Lemaitre Law) and is expressed as

$$v = H_0 d, \qquad\qquad\qquad\qquad (2.13)$$

where v is the recession velocity, d is the distance of the galaxy and H_0 is the Hubble constant. This shows a linear relation between the velocity and the distance of the galaxy and a constant rate of expansion given by H_0. The Hubble diagram shown in Fig. 2.1 is the graphical representation of Hubble's law. This suggest that time ago distant galaxies were closer to us, which supports the Big Bang Theory.

H_0 represents the constant expansion rate in all directions and its is the value of the Hubble parameter, $H(t) = (1/a)(da/dt)$, today. The scale factor , a, is a time dependent quantity that characterizes the expansion of the universe and the Hubble parameter measures how fast the scale factor changes. By convention, $a = 1$ today and the value of the Hubble Constant is parameterized by a dimensionless quantity h and is defined by

$$H_0 = 100 \, h \, \text{km s}^{-1} \text{Mpc}^{-1}, \qquad\qquad\qquad\qquad (2.14)$$

where Mpc is a megaparsec and is equal to 3.0856×10^{22} m. Since the measurement made by Hubble in 1929, the value of the Hubble Constant has changed and even today there is no consensus about its exact value, at the 5% level[5]. Observations of the Cepheids and supernovae[1,32], CMB[21,33], H_2O masers of accretion disks[34–36], quasars
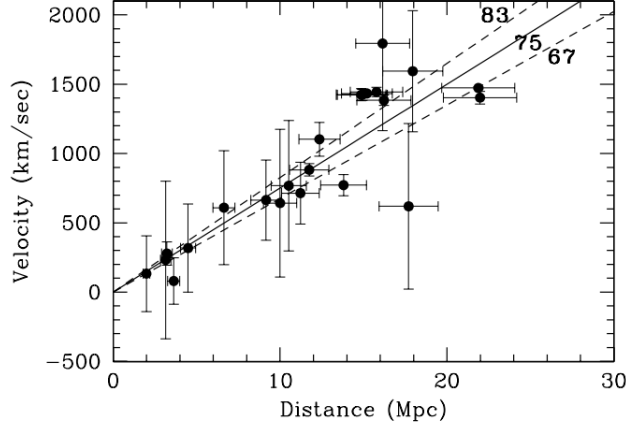
Figure 2.1: Hubble diagram from the Hubble Space Telescope Key project[1].

strongly lensed by galaxies[37–39] and the combined analysis of gravitational wave and electromagnetic data[40,41] have been used to measure the value of H_0. Now, the current value of h is about 0.7.

2.2.2 Big Bang Nucleosynthesis

Before Big Bang Nucleosynthesis (BBN), it was taken for granted that all the stars initiate their lives made out of hydrogen and the heavier elements formed through the nuclear reactions at their cores. Although it is true this is the via to generate heavy elements, the light elements (D,^{3}He, Li and especially ^{4}He) could not be produced in this way. Instead, the abundances of these elements seem to be from the primordial gas which gave rise to the stars. They were synthesized in the first three minutes of the Universe life which supports the Big Bang Cosmology[2,42,43].

BBN occured at the point were the temperature of the Universe was 1 MeV. At temperatures above this value, weak interactions were in thermal equilibrium. At that moment, the cosmic plasma consisted of photons, electrons, positrons, neutrinos and baryons. The ratio of baryons to photons is small,

$$\eta_b \equiv \frac{n_b}{n_\gamma} = 6.0 \times 10^{-10} \left(\frac{\Omega_b h^2}{0.022} \right), \tag{2.15}$$

where n_b and n_γ are the number density of baryos and photons, respectively.

At high temperatures, compared to nuclear binding energies, immediately after a nucleus is produced, it is destroyed by a high energy photon. Consider the deuterium production, $n + p \leftrightarrow D + \gamma$, at the equlibrium condition of weak interactions. The fraction of deuterium is given by[5]

$$\frac{n_D}{n_b} \sim \eta_b \left(\frac{T}{m_p} \right)^{3/2} e^{B_D/T}, \tag{2.16}$$

where T is the temperature, m_p is the proton mass, and B_D is the binding energy of deuterium and is equal to 2.22 MeV. Eq. (2.16) shows that the smallness of n_b inhibits nuclei production until T drops well below the nuclear binding energy. Then, at temperatures above 0.1 MeV, there are no nuclei and only free protons and neutrons exist.

Since there are are just free protons and neutros, we need to know in which ratio to find the nuclei they can form. Protons can be transformed to neutrons via weak interactions and the expression at equilibrium ratio is given by

$$\frac{n_p}{n_n} = e^{Q/T}, \tag{2.17}$$

where $Q \equiv m_n - m_p = 1.293$ MeV. Hence, at high temperatures, the ratio of protons and neutrons is around ~ 1. However, as the temperature drops below 1 MeV the amount of neutrons decreases. This amount would drop to zero if the weak interactions could work efficiently to maintain the equilibrium indefinitely. In the real world this is not the case.

The evolution of the ratio of neutrons to total nuclei, X_n, is given by

$$\frac{dX_n}{dt} = \lambda_{np}\left[(1 - X_n)e^{-Q/T} - X_n\right], \tag{2.18}$$

with

$$X_n \equiv \frac{n_n}{n_n + n_p}. \tag{2.19}$$

Fig. 2.2 shows the time-temperature evolution of $n_n/n_p = X_n/(1 - X_n)$. As the temperature decreases below ~ 1 MeV, weak interactions become too slow to maintain equilibrium and the n/p falls out of equilibrium. This ratio frezzes out at $\sim 1/7$ and at temperatures below 0.1 MeV the neutron decay and Deuterium production become important. This is the beginning of the BBN and the sharp drop at this level is the result of the Deuterium production.

At the point where decays become relevant, the time temperature relation is

$$t = 132s\left(\frac{0.1\text{MeV}}{T}\right)^2, \tag{2.20}$$

and at the moment light elements production (onset of BBN) the neutron abundances is[2]

$$X_n(T_{nuc}) = 0.11, \tag{2.21}$$

where $T_{nuc} \sim 0.07$ MeV is the temperature at which BBN begins.

Now that we know the fraction of neutrons at the beginning of BBN, we can turn to light element formation. Comparing helium to deuterium formation, the former is favored because its binding energy is larger than the binding energy of deuterium, recall the factor $e^{B/T}$. In fact, Fig. 2.3 exhibit that almost instantly after deuterium production, helium is produced. Practically all the remaining neutrons are used to form ^{4}He at $T \sim T_{nuc}$. The production of ^{4}He requires 2 neutrons, therefore, its abundance is equal to half the neutron abundance. The mass fraction of helium is given by
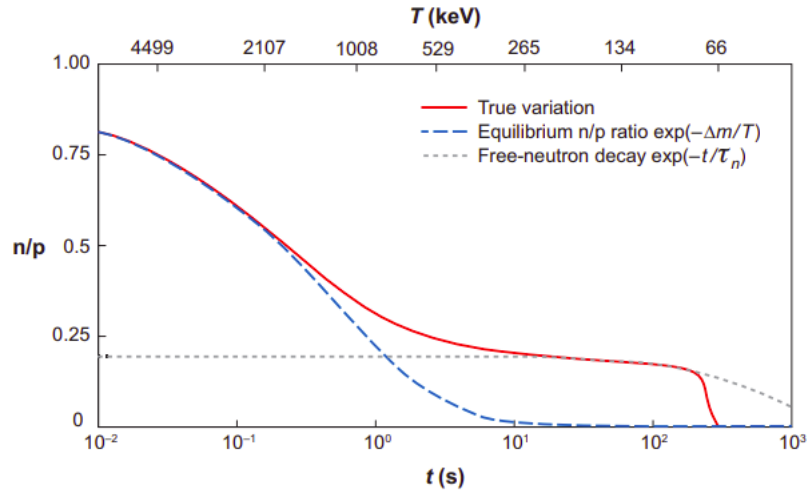
Figure 2.2: Evolution of neutronn to proton ratio. The solid curve shows the true variation, the dashed curve shows the equilibrium n/p ratio (with $\Delta m \equiv Q$) and the dotted curve shows the free-neutron decay [2].
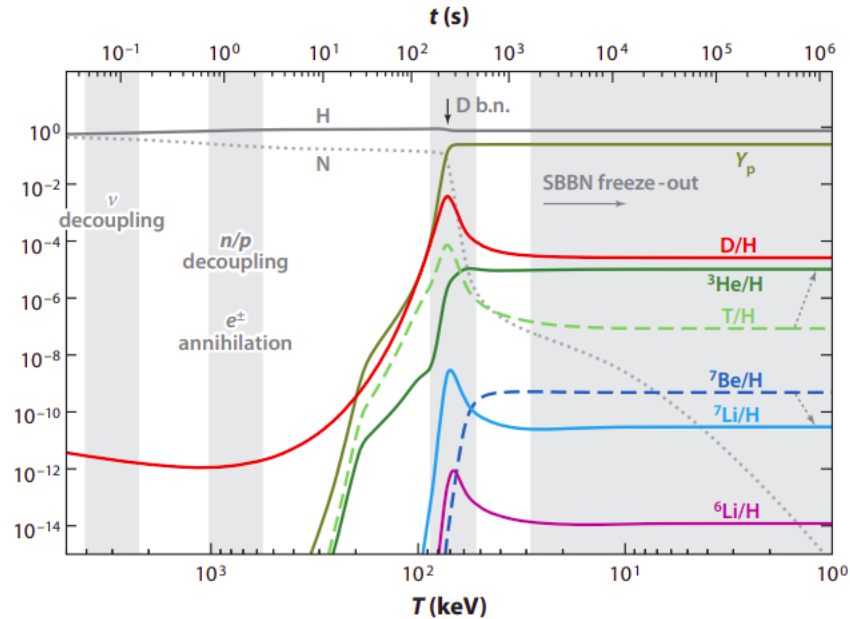

Figure 2.3: Time and temperature evolution of the mass fraction in light elements during the standard BBN. The gray vertical bands shows the main BBN stages [3].

$$Y_p \equiv \frac{4n(^4\mathrm{He})}{n_b} = 2X_n(T_{nuc}), \tag{2.22}$$

this yields $Y_p = 0.22$, which is in concordance with a full numerical calculation[44]

$$Y_p = 0.2262 + 0.01351 \ln(\eta_b/10^{-10}). \tag{2.23}$$

Then, from the total matter in the Universe $\sim 22\%$ of the matter is made up of ^{4}He. A track of a whole network of nuclear reactions allow us to calculate the abundances of the other nuclei. These contributions are deuterium $\sim 10^{-4}$, ^{3}He $\sim 10^{-5}$ and ^{7}Li 10^{-10} [27]. Remarkably, all these abundances can be measured and for that reason BBN is a powerful tool to tests the Hot Big Bang model.

2.2.3 Cosmic Microwave Background

During decoupling the mean free path of the photons increased to become virtually infinite. Then, the temperature of the photon-baryon fluid at that moment was transferred to the photons. After decoupling photons hardly interacted with matter, therefore its temperature could only change due to the redshift produced by the expansion of the Universe. As a consequence, the flux of photons that we see today in the CMB is the same flux arriving from the Last Scattering Surface (LSS). Given an homogeneous and isotropic Universe, the interaction of photons with electrons for the last time should occur, in average, at the same level for every point and in all directions of space. And this is exactly what an observer sees no matter its position, an homogeneous and isotropic distribution of photons.

Taking into account that the photon-baryon fluid was at thermal equilibrium, we could assume that energy distribution should be a Planck black body spectrum before decoupling. For a black body spectrum, the intensity of a gas of photons is given by

$$I_\nu = \frac{4\pi\hbar\nu^3/c^2}{exp[2\pi\hbar\nu/k_BT] - 1}, \tag{2.24}$$

where ν is its frequency, k_B is the Boltzmann constant and T is the temperature.

It is not too impressive that photons shows a perfect black body spectrum even after travelling billion of years and considering that they have no way to maintain in thermal equilibrium with its environment. Besides, the background radiation has an homogeneous temperature though it may seem strange because it was released not instantaneously and resulting in different redshifts and different initial temperatures. These things can be understood by taking a look at the energy density dependence on the temperature

$$\epsilon_r = \rho_r c^2 = \alpha T^4. \tag{2.25}$$

The frequency of radiation inversely scales with the scale factor, $\nu \sim 1/a$, due to the cosmic expansion. Besides, their energy density scales as: $\rho_r \sim 1/a^4$, so from Eq. (2.25): $T \sim 1/a$. Consequently, though all photons were not released at the same time, the photons released later at a lower temperature, experimented a bit less redshift compared with those released earlier. This effect compensates the possible difference in redshift and initial temperatures that
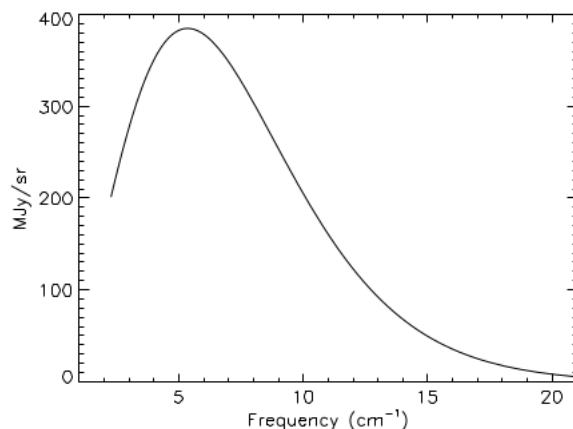
Figure 2.4: Intensity as a function of frequency of cosmic microwave radiation from FIRAS instrument[4]. The plot shows a black-body spectrum with $T_0 = 2.728$ K.

photons could have during decoupling. Since this predictions are based in a FRW Universe, the detection of the CMB and its features confirms that we live in such Universe. The volume of the Universe scale as: $1/a^3$, hence from Eq. (2.24) it can be realized that a Planck spectrum can be maintained in the expanding Universe and a decreasing temperature inversely proportional to a. Fig. 2.4 shows the extraordinary agreement between the black-body spectrum prediction of the Big Bang and the observations made by Far-InfraRed Absolute Spectrophotometer (FIRAS) instrument on the COBE satellite[4].

During the first 25 years of studying the CMB, no anisotropies were detected, which pointed out to a smooth universe. This interval of time solidified the idea of a smooth Big Bang. However, in 1992 COBE satellite reported the discovery of anisotropies in the CMB [17,45] which suggested a not fully smooth universe. The fractional temperature fluctuations founded in the cosmic plasma were of the order of 10^{-5}.

2.3   Issues with the Big Bang

2.3.1   Horizon problem

According to observations, when the universe had 380,000 years, it was very smooth to about 10^{-5}. Besides, photons and baryons were extraordinarily close to thermal equilibrium. However, the reason for this was not clear because if we take a random patch of the size of the observable universe, this should be inhomogeneous to a high level. Now, a possible explanation could be inhomogeneous, then if the universe began being highly inhomogeneous by letting be in contact, after some time it eventually will reach an equilibrium point to share the same temperature. To see if this scenario is possible, it is useful to introduce the conformal time
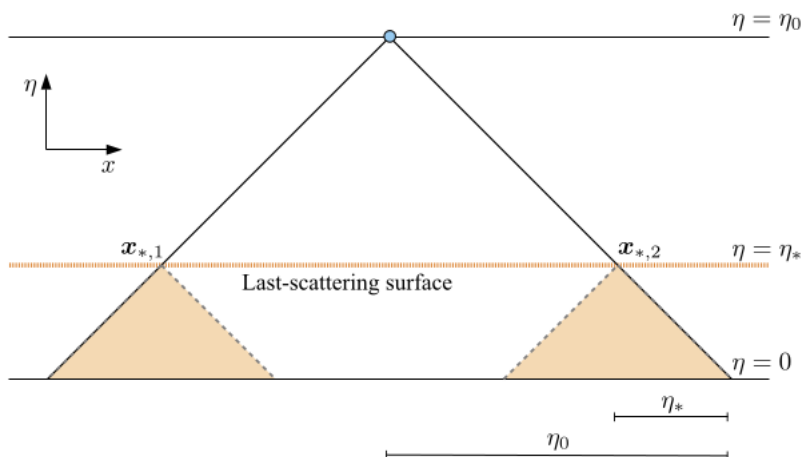
Figure 2.5: The horizon problem[5]. An observer at the top (blue dot) receives light signals coming from his past light cones. The cone intersects the LSS at $\eta = \eta_*$ and the CMB is emitted and found to be uniform. Only signals coming from the shaded region below $x_{*,1}$ and $x_{*,2}$ can influence this CMB photon, however, these regions do not overlap.

$$\eta(t) = \int_0^t \frac{dt'}{a(t')}, \tag{2.26}$$

it is the comoving distance that light could travel starting at $t = 0$. Taking a look to Fig. 2.5 gives the impression that this solution do not work, since the observations of the CMB shows that different parts of the universe were so distant at time of decoupling that they could not be in causal contact with one another. Hence, the idea of thermalization seems impossible.

This problem can be shown by finding the comoving horizon η at recombination, that is, the comoving distance light is able to travel from $\eta = 0$ to η_*. After that, we can check if this is able to join different patches of the CMB that we see today. Assuming that only matter and radiation are present in the universe and going back to $t = 0$, the comoving horizon at recombination is $\eta = (a) \equiv 281 h^{-1}$ Mpc[5]. Looking the CMB today, the comoving distance between two points apart by a small angle θ is

$$\chi(\theta) \simeq \chi_* \theta = (\eta_0 - \eta_*)\theta. \tag{2.27}$$

Since $\eta_0 \approx 14200 h^{-1}$ Mpc, then we can conclude that two points in the CMB separated by

$$\theta \geq \frac{\eta_*}{\eta_0 - \eta_*} \approx 1.2°, \tag{2.28}$$

are not able to be in thermal contact at recombination. The difference between η_0 and η_* is larger than Fig. 2.5 suggest, the difference is of the order of 50, so this aggravates the problem. An assumption of what underlies the

problem is obtain by rewriting Eq. (2.26) and changing the integration variables from t' to $\ln a'$

$$\eta(a) = \int_0^a d\ln a' \frac{1}{a' H(a')}.$$
(2.29)

Now, it becomes in the logarithmic integral of the comoving Hubble radius ($1/aH$), which is the distance that light travels during one expansion time. This gives a measuring rod to evaluate if photons or baryons can communicate within one e-fold of expansion. For a matter dominated universe or a radition dominated universe, H evolves as $a^{-3/2}$ or a^{-2}. Then, we get a Hubble radius that is always increasing, in which case the largest contribution to η is given by the most recent epochs.

2.3.2 Flatness problem

To see the flatness problem, consider the Friedmann equations (Eq. (2.4) and Eq. (2.5)) and neglet the cosmological constant, then one can obtain he evolution equation for the curvature density

$$\Omega_k =\equiv -\frac{k}{a^2 H^2} = 1 - \Omega,$$
(2.30)

where $\Omega \equiv 8\pi\rho/(3H^2)$. Then, one can find

$$\frac{d\Omega_k}{d\ln a} = (3w + 1)(1 - \Omega_k)\Omega_k,$$
(2.31)

remember, $w = P/\rho$ is the equation of state parameter. Now, one can integrate Eq. (2.31), when w is constant, and obtain

$$\frac{\Omega_{k0}}{\Omega_k(a)} = (1 - \Omega_{k0})\left(\frac{a}{a_0}\right)^{(-1-3w)} + \Omega_{k0},$$
(2.32)

where Ω_{k0} is the curvature today. The observations[46] constrain $|\Omega - 1| \lesssim 0.01$ and one can find that at radiation-matter equality

$$|\Omega(a_{eq}) - 1| \lesssim 3 \times 10^{-6},$$
(2.33)

and at the Planck time,

$$|\Omega(a_p) - 1| \lesssim 10^{-60}.$$
(2.34)

Since radiation, non relativistic matter and curvature evolve as a^{-4}, a^{-3} and a^{-2}, respectively, then curvature should eventually dominates. However, today it does not dominate, so it should very negligible in the past. The ΛCDM model can not explain why the spatial curvature is so small.

2.4   Inflation

Inflation is a period of the universe that occurs before the hot big bang history. Information from the BBN suggest that the radiation dominated era was at $t \sim 1 - 100$ sec, therefore, inflation should occur at least earlier than this[47]. Furthermore, the dominant form of energy during inflation needs to have $w \simeq -1$ or $H \simeq$ const. Via the Friedmann equations one can find three equivalent conditions that are needed for inflation.

The first condition is a decreasing comoving horizon. A shrinking Hubble sphere is defined as

$$\frac{d}{dt}\left(\frac{1}{aH}\right) < 0, \tag{2.35}$$

this relation is fundamental to solve the horizon and flatness problems, besides, it is key for the mechanism to generate fluctuations.

The second condition is the definition of inflation itself, an era of repulsive gravity. From Eq. (2.35)

$$\frac{d}{dt}(aH)^{-1} = \frac{-\ddot{a}}{(aH)^2}, \tag{2.36}$$

from this we can see that a shrinking comoving Hubble radius results in an accelerated expansion

$$\frac{d^2a}{dt^2} > 0. \tag{2.37}$$

The third condition is the existence of a material with a negative pressure. To have an accelerated expansion we need

$$p < -\frac{1}{3}\rho, \tag{2.38}$$

where p is the pressure and ρ is the energy density, i,e., we need a negative pressure.

The number of e-folds, N measures the amount of expansion during inflation and is given by[48]

$$N(t) \equiv \ln\left[\frac{a(t)}{a_i}\right], \tag{2.39}$$

where a_i is the scale factor at the begining of inflation.

2.4.1   Horizon problem's solution

Inflation solves in an easy way the horizon problem if the number of e-folds is sufficiently large. In fact, the primordial phase of inflation can explain why regions of the CMB that seems to be causally disconnected at recombination share almost the same temperature. Assuming an exponential expansion during inflation,

$$a(t) = a_i e^{H\Delta t}, \tag{2.40}$$

then, one can compute the number of e-folds needed to solve the horizon problem. We have that our current observable Universe, d_{H_0}, has to be smaller at the end of inflation than the size of a causal region at the beginning of inflation[48] d_{H_i}, then

$$d_{H_0}(t_0)\frac{a_{end}}{a_0} < d_{H_i}\frac{a_{end}}{a_i} = d_{H_i}(t_i)e^N, \tag{2.41}$$

here, a_{end} is the scale factor at the end of inflation. If inflation ends at the Grand Unification scale ($\rho_{end}^{1/4} \sim 10^{16}$ GeV), assuming

$$d_{H_i}(t_i) \sim \frac{l_{Pl}T_{Pl}}{T_{end}}, \tag{2.42}$$

where T_{Pl} and l_{Pl} are the the Planck temperature and the Planck length, respectively. Then, one needs

$$N \sim \ln\left[\frac{T_0 d_{H_0}(t_0)}{T_{end} d_{H_i}(t_i)}\right] \gtrsim 57, \tag{2.43}$$

where T_0 is the current photon temperature. If this condition is satisfied, one can conclude that the entire observable Universe emerges out of the same causal region before the beginning of inflation.

2.4.2 Flatness problem's solution

Consider the curvature density

$$\Omega_k \equiv -\frac{k}{a^2 H^2} = 1 - \Omega, \tag{2.44}$$

to decrease Ω_k, we need an epoch of the universe in which $1/aH$ decreases with time. As already mentioned the condition for $(aH)^{-1}$ to decrease with time is to have an accelerate expansion,

$$\frac{d}{dt}\left(\frac{1}{aH}\right) < 0 \qquad \Rightarrow \qquad \ddot{a} > 0. \tag{2.45}$$

If the $1/aH$ decreases this leads the universe toward flatness. Furthermore, from the exponential growth at inflation, we have

$$|\Omega - 1| \propto e^{-2Ht}, \tag{2.46}$$

and one can immediately see that the difference $|\Omega - 1|$ tends to zero exponentially with time. This allows an extremely flat Universe. If we assume $H \simeq 1$ during inflation, one has

$$|\Omega_k(a_{end})| = |\Omega_k(a_i)|e^{-2N}, \tag{2.47}$$

and assuming at the Planck scale a curvature of the order of unity and with $N \gtrsim 70$, then, the flatness problem is naturally solved.

2.5 The Physics of Inflation

2.5.1 Scalar field dynamics

The simplest model capable of driving a period of inflation involve a single scalar field ϕ, the inflaton. The dynamics of a scalar field coupled to gravity has the following action [49]

$$S = \int d^4x \sqrt{-g} \left[\frac{1}{2}R + \frac{1}{2}g^{\mu\nu}\partial_\mu\phi\partial_\nu\phi - V(\phi) \right] = S_{EH} + S_\phi. \tag{2.48}$$

The first term is the gravitational Einstein-Hilbert action, S_{EH} and the other two terms are action of a scalar field, S_ϕ. The self interactions of the scalar field are described by the potential, $V(\phi)$. The energy momentum tensor of ϕ is

$$T_{\mu\nu}^{(\phi)} \equiv -\frac{2}{\sqrt{-g}}\frac{\delta S_\phi}{\delta g^{\mu\nu}} = \partial_\mu\phi\partial_\nu\phi - g_{\mu\nu}\left[\frac{1}{2}\partial^\sigma\phi\partial_\sigma\phi + V(\phi) \right], \tag{2.49}$$

and the field equation of motion is

$$\frac{\delta S_\phi}{\delta\phi} = \frac{1}{\sqrt{-g}}\partial_{mu}(\sqrt{-g}\partial^\mu\phi) + V' = 0, \tag{2.50}$$

where $V' = \frac{dV}{d\phi}$. Assuming FRW metric of Eq. (2.1) and for a homogeneous field configuration, the energy density and pressure are

$$\rho = \frac{1}{2}\dot{\phi}^2 + V, \tag{2.51}$$

$$p = \frac{1}{2}\dot{\phi}^2 - V. \tag{2.52}$$

Therefore the equation of state is

$$w = \frac{p}{\rho} = \frac{\frac{1}{2}\dot{\phi}^2 - V}{\frac{1}{2}\dot{\phi}^2 + V}. \tag{2.53}$$

If the potential energy dominates the kinetic energy, we have a negative pressure ($w < 0$) and consequently an accelerated expansion. The dynamics of the scalar field is given by

$$\ddot{\phi} + 3H\dot{\phi} = -V', \qquad \text{and} \qquad H^2 = \frac{1}{3}\left[\frac{1}{2}\dot{\phi}^2 + V(\phi) \right]. \tag{2.54}$$

Large values of the potential leads to significant Hubble friction from the term $H\dot{\phi}$

2.5.2 Slow-roll Inflation

A Universe dominated by a scalar field has an acceleration equation with the form

$$\frac{\ddot{a}}{a} = -\frac{1}{6}(\rho + 3p) = H^2(1 - \epsilon), \tag{2.55}$$

where

$$\epsilon \equiv \frac{3}{2}(w + 1) = \frac{1}{2}\frac{\dot{\phi}^2}{H^2}, \tag{2.56}$$

it is known as slow-roll parameter and it is related to the the evolution of the Hubble parameter

$$\epsilon = -\frac{\dot{H}}{H^2}. \tag{2.57}$$

If $\epsilon < 1$, then it leads to an accelerated expansion. The de Sitter limit, $p \to -\rho$ leads to $\epsilon \to 0$ and the potential energy dominates over kinetic energy

$$\dot{\phi}^2 \ll V(\phi). \tag{2.58}$$

To have a sustained accelerated expansion the second time derivative of ϕ has to be small enough

$$|\ddot{\phi}| \ll |3H\dot{\phi}|, \; |V'(\phi)|. \tag{2.59}$$

This condition requires the second slow-roll parameter to be small

$$\eta = -\frac{\ddot{\phi}}{H\dot{\phi}} = \epsilon - \frac{1}{2\epsilon}\frac{d\epsilon}{dN}, \tag{2.60}$$

and $|\eta| < 1$ ensures a small change of ϵ per e-fold. The slow-roll conditions can also be expressed in term of the potential

$$\epsilon_V = \frac{M_{Pl}^2}{2}\left(\frac{V'}{V}\right)^2, \tag{2.61}$$

and

$$\eta_V = M_{Pl}^2\left(\frac{V''}{V}\right), \tag{2.62}$$

In the slow-roll regime

$$\epsilon_V \ll 1 \qquad \text{and} \qquad |\eta_V| \ll 1. \tag{2.63}$$

and the background evolution is

$$H^2 \approx \frac{V(\phi)}{3M_{Pl}}, \tag{2.64}$$

$$\dot{\phi} \approx -\frac{V'(\phi)}{3H}, \tag{2.65}$$

and the spacetime is approximately de Sitter

$$a(t) \sim e^{Ht}. \tag{2.66}$$

The number of e-folds before inflation ends is

$$N(t) = \ln\frac{a(t_{end})}{a(t)}, \tag{2.67}$$

where t_{end} is the time at the end of the inflation. This can be expressed in terms of the scalar field potential:

$$N = \int_t^{t_{end}} H\,dt \simeq \frac{1}{M_{pl}} \int_{\phi_{end}}^{\phi} \frac{V}{V'}d\phi, \tag{2.68}$$

or

$$N = \int_{\phi_{end}}^{\phi} \frac{d\phi}{\sqrt{2\epsilon}} \approx \int_{\phi_{end}}^{\phi} \frac{d\phi}{\sqrt{2\epsilon_V}}. \tag{2.69}$$

2.6 The CMB temperature power spectrum

CMB exhibits an almost perfect black-body spectrum at a temperature of $2.72K$. It provides a lot of information about the universe and the vast majority of information lies in its temperature field. Although across the celestial sphere the average temperature is amazingly uniform, there are small fluctuations at the level of 10^{-5}. The deviations from the average temperature are defined by[50]

$$\Theta(\hat{n}) = \frac{\delta T(\hat{n})}{T} = \frac{T(\hat{n}) - \langle T \rangle}{\langle T \rangle}, \tag{2.70}$$

where $\hat{n}$ is the direction of the signals in the sky $\hat{n} = (\theta, \phi)$.

Since temperature fluctuations are projected in a 2D spherical surface, spherical harmonics are used to expand the temperature field. The spherical harmonics are defined as

$$Y_{lm} = \sqrt{\frac{2l + 1(l - m)!}{4\pi(l + m)!}} P_l^m(cos\theta)e^{im\phi}, \tag{2.71}$$

where P_l^m are the Legendre polynomials and the indices $l = 0, 1, ..., \infty$ and $l \leq m \geq l$. They form a complete orthonormal set. l is called the multipole and constitutes a given angular scale in the sky surface α, with $\alpha = 180^0/l$.

Temperature fluctuations field are expanded using these functions

$$\Theta(\hat{n}) = \sum_{l=0}^{l=\infty} \sum_{m=-l}^{l} a_{lm} Y_{lm}(\hat{n}), \tag{2.72}$$

where,

$$a_{lm} = \int_{\theta=-\pi}^{\pi} \int_{\phi=0}^{2\pi} \Theta(\hat{n}) Y_{lm}^*(\hat{n}) d\Omega.$$ (2.73)

Average over an isotropic on average Universe and random field of temperature fluctuations, have the property

$$\langle a_{lm} a_{l'm'}^* \rangle = \delta_{ll'} \delta_{mm'} C_l^T,$$ (2.74)

where the delta functions arises from isotropy and the coefficient C_l depends only on the total angular momentum l. We know only one universe, then, we can study only one set of coefficients a_{lm}. Assuming the validity of Eq. (2.74), one can obtain the the coefficients C_l from observations [51]

$$C_l^T = \frac{1}{2l+1} \sum_{m=-l}^{l} |a_{lm}|^2.$$ (2.75)

There is an unavoidable error in the estimation of any given C_l^T of $\triangle C_l^T = \sqrt{2/(2l+1)}$, This is known as the cosmic variance.

A two-point correlation function of the temperature fluctuation is determined by the coefficients C_l. From (Eq. 2.70), the two point function is given by

$$\langle \delta T(\hat{n_1}) \, \delta T(\hat{n_2}) \rangle = T^2 \sum_l \frac{2l+1}{4\pi} C_l \cdot P_l(\hat{n_1}\hat{n_2}).$$ (2.76)

The variance of temperature is obtained from Eq. (2.76),

$$\langle \delta T(\hat{n}) \rangle = T^2 \sum_l \frac{2l+1}{4\pi} C_l \approx T^2 \int d\log l \frac{(l+1)l}{2\pi} C_l,$$ (2.77)

where the last equality holds for large l. Hence, the amplitude squared of the temperature fluctuation in a decimal interval of multipoles is given by

$$\mathcal{D}_l \equiv T^2 \frac{l(l+1)}{2\pi} C_l.$$ (2.78)

Fig. 2.6 shows results of the measurements of CMB temperature anisotropy made by different experiments [6].

2.6.1   Cosmological perturbations

The power spectrum is useful to characterize the properties of the fluctuations of the inflaton. The power spectrum of tensor and scalar expands around a pivot scale defined by k_* , and it parameterizes by

$$P_{\mathcal{R}}(k) = A_s \left(\frac{k}{k_*} \right)^{n_s - 1 + \frac{1}{2} dn_s/d\ln k \ln(k/k_*) + \frac{1}{6} d^2 n_s/d\ln k^2 (\ln(k/k_*))^2 + \dots}, $$ (2.79)

$$P_t(k) = A_t \left(\frac{k}{k_*} \right)^{n_t + \frac{1}{2} dn_s/d\ln k \ln(k/k_*) + \dots}, $$ (2.80)
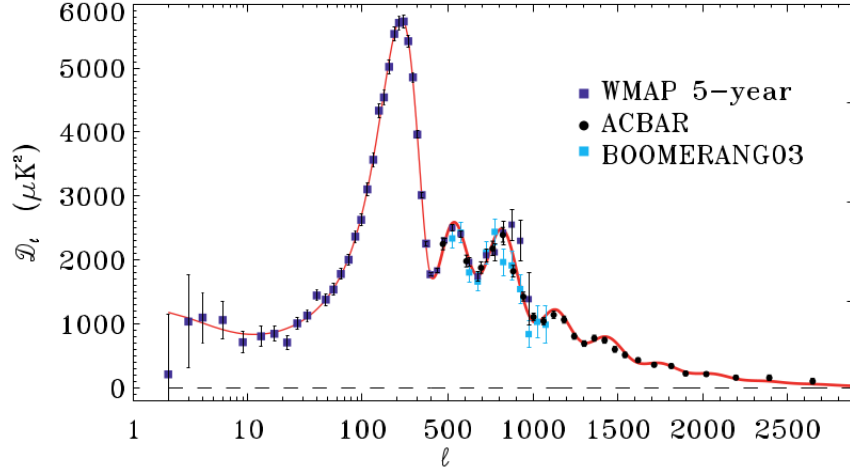
Figure 2.6: CMB temperature anisotropy from WMAP, BOOMERANG and ACBAR experiments[6].

where A_s , A_t is the scalar, tensor amplitude respectively. On the other hand, the tensor and scalar spectral indices and their running terms are given by

$$n_t(k) \simeq -2\epsilon_v, \tag{2.81}$$

$$n_s(k) \simeq 1 - 6\epsilon_v + 2\eta_v, \tag{2.82}$$

$$\frac{dn_t(k)}{dn \ln k} \simeq 4\eta_v - 8\epsilon_v^2, \tag{2.83}$$

$$\frac{dn_s(k)}{dn \ln k} \simeq 16\eta_v\epsilon_v - 24\epsilon_v^2 - 2\xi_v^2, \tag{2.84}$$

$$\frac{d^2 n_s(k)}{dn \ln k^2} \simeq 192\epsilon_v^3 - 192\epsilon_v^2\eta_v + 32\epsilon_v\eta_v^2 + 24\epsilon_v\xi_v^2 - 2\eta_v\xi_v^2 - 2\varpi_v^3, \tag{2.85}$$

where

$$\xi_v^2 = \frac{M^4 V'(\phi)V'''(\phi)}{V^2(\phi)}, \quad \text{and} \quad \varpi_v^3 = \frac{M^6 V'^2(\phi)V''''(\phi)}{V^3(\phi)}. \tag{2.86}$$

The tensor-scalar ratio is given by

$$r = \frac{P_t(k_*)}{P_\mathcal{R}(k_*)} \simeq 16\epsilon_v \simeq -8n_t. \tag{2.87}$$

2.7   Chaotic Potential with a step

In 1983, Linde proposed a scenario where inflation may emerge from chaotic initial conditions in the early universe[52]. A power law potential used in this scenario is

$$V(\phi) = \mathsf{g}\phi^n, \qquad n > 0, \tag{2.88}$$

where g is the coupling and has dimension

$$[\mathsf{g}] = (\text{mass})^{4-n}. \tag{2.89}$$

This scenario is also called "chaotic inflation", due to the nature of the initial conditions which allow inflation. Since in this work we use only the second power of this potential, we call it "chaotic potential"

$$V(\phi) = \frac{m^2}{2}\phi^2, \tag{2.90}$$

where ϕ is the inflaton field. Now, the step is modeled by assuming the potential

$$V(\phi) = \frac{1}{2}m^2\phi^2\left[1 + c\tanh\left(\frac{\phi - \phi_{\text{step}}}{d}\right)\right]. \tag{2.91}$$

From Eq. (2.51) and Eq. (2.52) we find the energy density and pressure

$$\rho = \frac{1}{2}\dot\phi^2 + \frac{1}{2}m^2\phi^2\left[1 + c\tanh\left(\frac{\phi - \phi_{\text{step}}}{d}\right)\right], \tag{2.92}$$

and

$$\rho = \frac{1}{2}\dot\phi^2 - \frac{1}{2}m^2\phi^2\left[1 + c\tanh\left(\frac{\phi - \phi_{\text{step}}}{d}\right)\right]. \tag{2.93}$$

From Eq. (2.54), the dynamics of the scalar field is determined by

$$H^2 = \frac{1}{3}\left\{\frac{1}{2}\dot\phi^2 + \frac{1}{2}m^2\phi^2\left[1 + c\tanh\left(\frac{\phi - \phi_{\text{step}}}{d}\right)\right]\right\}, \tag{2.94}$$

and

$$\ddot\phi + 3H\dot\phi = -m^2\phi\left[1 + c\tanh\left(\frac{\phi - \phi_{\text{step}}}{d}\right) + 2dc\phi\,\text{sech}^2\left(\frac{\phi - \phi_{\text{step}}}{d}\right)\right]. \tag{2.95}$$

And there is no analytical solution for ϕ.

2.8 CAMB

In this work, it was used the Code for Anisotropies in the Microwave Background (CAMB). It is a Python and Fortran code based on CMBFast. CAMB is used to compute different things related to the CMB radiation such as the CMB itself, CMB lensing, transfer functions and matter power spectra, and background cosmological functions[53]. It is a powerful tool that is used by many papers[54–56]. It works by providing initial conditions, quantum fluctuations and inflation gives rise to primordial perturbations. In CAMB the natural logarithm of the scalar and tensor power spectra is

$$\ln P_s = \ln A_s + (n_s - 1)\ln\left(\frac{k}{k_s}\right) + \frac{n_{\text{run}}}{2}\left[\left(\frac{k}{k_s}\right)\right]^2 + \frac{n_{\text{run,run}}}{6}\left[\left(\frac{k}{k_s}\right)\right]^3, \tag{2.96}$$

and

$$\ln P_t = \ln A_t + n_t\ln\left(\frac{k}{k_t}\right) + \frac{n_{t,\text{run}}}{2}\left[\left(\frac{k}{k_s}\right)\right]^2, \tag{2.97}$$

where A_s and A_t are the scalar power amplitude and tensor tensor power amplitude, respectively. They determine the variance of the primordial density and gravitational wave fluctuations. The pivot scale, k_s, is the scale best constrained by a given set of observations. The scalar spectral index, n_s, relates the change in density fluctuations with the scale. The running terms of the spectral index are n_{run} and $n_{\text{run,run}}$.

In this work we need to obtain the angular power spectrum, therefore, we need

$$\mathcal{D}_l \equiv T^2\frac{l(l+1)}{2\pi}C_l. \tag{2.98}$$

This code use input parameters which are defined in a "params.ini". This file have to contain all information about the cosmology (cosmological parameter values, etc). Besides, we can ask to output the observables of interest by specifying it in the "params.ini" file. Fig. 2.7 shows an example of this type of files.

There are several output files that CAMB can generate, but the file used for this work looks like the one in Fig. 2.8. In this work the first two columns are used to obtain the angular power spectrum. In the first column is the multipole moment, l, and in the second column is the amplitude of the power spectrum, $\mathcal{D}_l$. The other columns are the polarization and temperature-polarization cross-correlation power spectra.

```
 1 #Parameters for CAMB
 2
 3 #output_root is prefixed to output file names
 4 output_root = test_tens
 5
 6 #What to do
 7 get_scalar_cls = T
 8 get_vector_cls = F
 9 get_tensor_cls = T
10 get_transfer   = F
11
12 #if do_lensing then lens_potential_output_file contains the unlensed CMB and lensing potential power spectra
13 #and lensed CMB Cls (without tensors) are in lensed_output_file, total in lensed_total_output_file.
14 do_lensing     = T
15
16 # 0: linear, 1: non-linear matter power (HALOFIT), 2: non-linear CMB lensing (HALOFIT),
17 # 3: both non-linear matter power and CMB lensing (HALOFIT)
18 do_nonlinear = 0
19
20 #Maximum multipole and k*eta.
21 #  Note that C_ls near l_max are inaccurate (about 5%), go to 50 more than you need
22 #  Lensed power spectra are computed to l_max_scalar-100
23 #  To get accurate lensed BB need to have l_max_scalar>2000, k_eta_max_scalar > 10000
24 #  To get accurate lensing potential you also need k_eta_max_scalar > 10000
25 #  Otherwise k_eta_max_scalar=2*l_max_scalar usually suffices, or don't set to use default
26 l_max_scalar       = 2200
27 #k_eta_max_scalar  = 4000
28
29 #  Tensor settings should be less than or equal to the above
30 l_max_tensor       = 1500
31 k_eta_max_tensor  = 3000
32
33 #Main cosmological parameters, neutrino masses are assumed degenerate
34 # If use_phyical set physical densities in baryons, CDM and neutrinos + Omega_k
35 use_physical   = T
36 ombh2          = 0.0226
37 omch2          = 0.112
38 omnuh2         = 0.00064
39 omk            = 0
40 hubble         = 70
41
42 #effective equation of state parameter for dark energy
43 w              = -1
```

Figure 2.7: Example of a file that contains the cosmological information need by CAMB.

```
#    L      TT              EE              TE              PP              TP
     2   0.246874E+03    0.118990E-01    0.792662E+00    0.252699E+06    0.681800E+04
     3   0.233256E+03    0.197687E-01    0.989601E+00    0.388864E+06    0.816793E+04
     4   0.219705E+03    0.226798E-01    0.102083E+01    0.509951E+06    0.882481E+04
     5   0.209017E+03    0.205953E-01    0.951909E+00    0.616954E+06    0.910322E+04
     6   0.201218E+03    0.156270E-01    0.834457E+00    0.711426E+06    0.916525E+04
     7   0.195824E+03    0.102248E-01    0.701750E+00    0.795222E+06    0.909988E+04
     8   0.192191E+03    0.601621E-02    0.573777E+00    0.869858E+06    0.895626E+04
     9   0.190184E+03    0.350528E-02    0.462897E+00    0.936648E+06    0.875999E+04
    10   0.189159E+03    0.238230E-02    0.373976E+00    0.996478E+06    0.853848E+04
    11   0.188932E+03    0.202371E-02    0.309829E+00    0.105045E+07    0.831305E+04
    12   0.189574E+03    0.190214E-02    0.270065E+00    0.109880E+07    0.808516E+04
    13   0.190703E+03    0.175487E-02    0.250977E+00    0.114268E+07    0.786730E+04
    14   0.192130E+03    0.155014E-02    0.247854E+00    0.118212E+07    0.765291E+04
    15   0.193876E+03    0.136328E-02    0.255749E+00    0.121794E+07    0.744528E+04
    16   0.195997E+03    0.126901E-02    0.270609E+00    0.125028E+07    0.724374E+04
    17   0.198374E+03    0.126658E-02    0.287068E+00    0.127950E+07    0.704842E+04
    18   0.200541E+03    0.133328E-02    0.302365E+00    0.130600E+07    0.685976E+04
    19   0.203688E+03    0.144013E-02    0.319178E+00    0.132996E+07    0.667626E+04
    20   0.206488E+03    0.154687E-02    0.331865E+00    0.135149E+07    0.649653E+04
    21   0.209566E+03    0.165501E-02    0.342954E+00    0.137086E+07    0.632175E+04
    22   0.212820E+03    0.179215E-02    0.351788E+00    0.138835E+07    0.615324E+04
    23   0.215850E+03    0.197629E-02    0.360295E+00    0.140409E+07    0.599039E+04
    24   0.219002E+03    0.222496E-02    0.370426E+00    0.141815E+07    0.583249E+04
    25   0.222468E+03    0.253254E-02    0.377160E+00    0.143066E+07    0.568027E+04
                                                                              1,1
```

Figure 2.8: Output file from CAMB.

Chapter 3

Results & Discussion

As mentioned, the Cosmic Microwave Background (CMB) shows an almost perfect black body distribution, with a temperature of $T = 2.72548 \pm 0.001$ K. However, the are temperature anisotropies over the celestial sphere. The dipole anisotropy is the strongest at the level of $\delta T/T \sim 10^{-3}$, this anisotropy is generated due to the motion of the Earth respect to the reference frame of the CMB. While the remaining anisotropies are at the level of $\delta T/T \sim 10^{-4} - 10^{-5}$. The temperature power spectrum shows these temperature anisotropies along the celestial sky. The power spectrum can be divided in three main regions: large angular scales ($l \lesssim 100$), intermediate angular scales ($l \lesssim 1000$) and large angular scales($l \gtrsim 1000$). As we will see, each of these three regions are affected to a different extent by a specific physical process.

The present chapter introduces the different power spectra obtained with a chaotic inflationary potential with a step in the slow-roll approximation by changing the values of parameters present in this potential. Later, the analysis of the mentioned three different regions are analyzed separately. Finally, the method used to obtain the tensor and spectral indices and their running terms, as well as the results obtained using the Code for Anisotropies in the Microwave Background (CAMB).

3.1 Scalar power spectra for a chaotic inflationary potential with a step into a slow-roll approximation

CMB anisotropies at the level of $\delta T/T \sim 10^{-5}$ have an extraordinary importance for cosmology. These anitropies carry important information about cosmological perturbations from the epoch of recombination and properties of the Universe after last scattering. The scalar power spectrum shows these anisotropies at different angular scales. The potential used in this work is

$$V(\phi) = \frac{1}{2}m^2\phi^2\left[1 + c\tanh\left(\frac{\phi - \phi_{\text{step}}}{d}\right)\right].$$

(3.1)

Different values were given to the parameters c, d, and ϕ_{step} in order to obtain different spectra and find the one that fits best to the data of Planck mission[23].

(a)   (b)

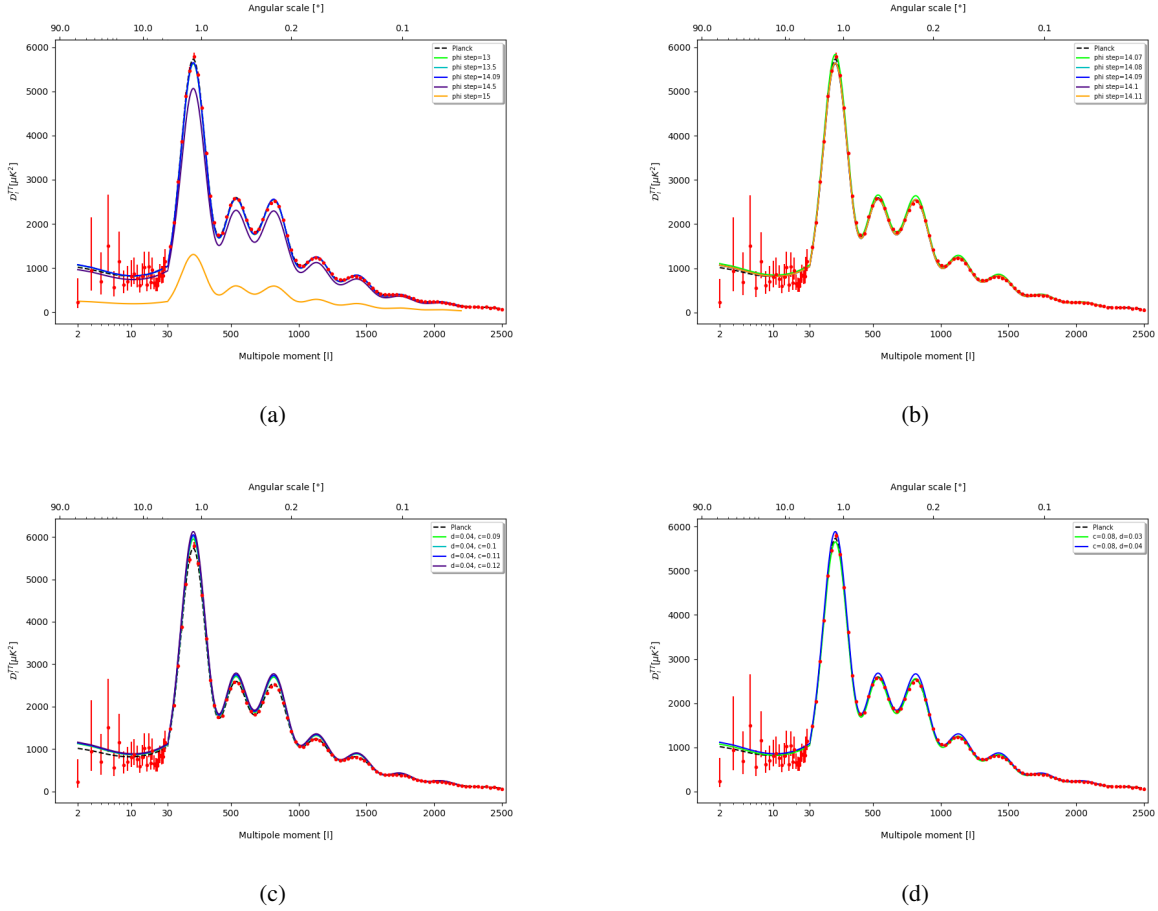(c)   (d)

Figure 3.1: Power spectrum obtained using the chaotic potential with a step. The black dashed line shows the best-fit reported from Planck data. The rest of the lines shows the power spectrum obtained with the chaotic potential with a step by changing the value of the parameters. In (a) and (b) changes the value of ϕ_{step}, in (c) changes the value of c and in (d) changes the value of d. The multipole moment for $2 < l < 29$ is represented in logarithmic scale.

The data of Planck mission is used for comparison because it is the more recent data compare to Cosmic Background Explorer (COBE) and Wilkinson Microwave Anisotropy Probe (WMAP) data. Fig. 3.1a, Fig. 3.1b Fig. 3.1c and Fig. 3.1d show the different power spectra obtained by changing the values of ϕ_{step}, c and d. Fig. 3.1a shows that for certain values of ϕ_{step} (14.5 and 15) the power spectrum obtained using Eq. (3.1) is far below from the spectrum obtained using Planck data. The power spectra of Fig. 3.1c and Fig. 3.1d look similar to the spectrum from Planck data for the values chosen for the parameters c and d.

3.1.1   Relative error

The validity of a model can be judged by the goodness of fit to the data[19]. Then, in order to assessed the goodness of fit, it has been computed the relative error and the percentage error is shown in Fig. 3.2b.
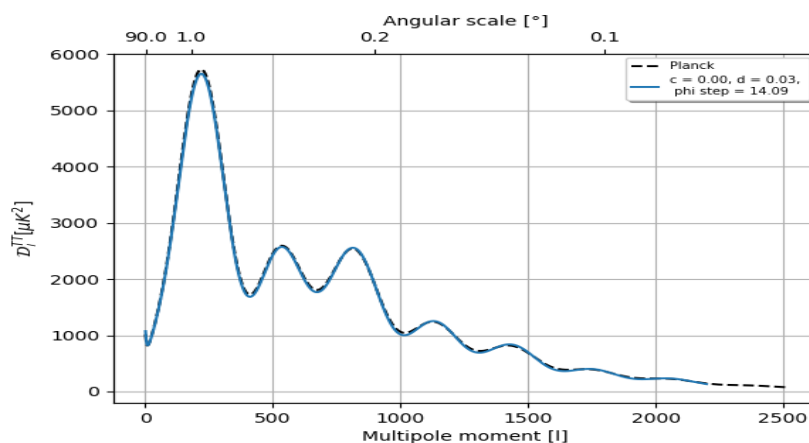
(a) Angular power spectrum
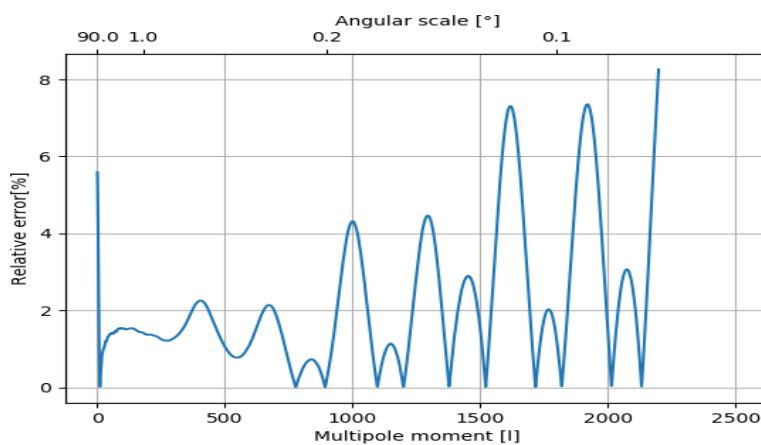
(b) Percentage error

Figure 3.2: (a) Angular power spectrum and (b) percentage error of the temperature power spectrum obtained from the chaotic potential with a step. The relative error is respect to the Planck data.

From all the values used to reproduce the temperature power spectrum with the potential $V(\phi)$ of Eq. (3.1), the ones that produced the lower relative error with respect to the Planck data are: $c = 0.08$, $d = 0.03$ and $\phi_{step} = 14.09$. Fig. 3.2b shows the percentage error, and one can see that along all the spectrum the difference between our model and the Planck data is below 9%.
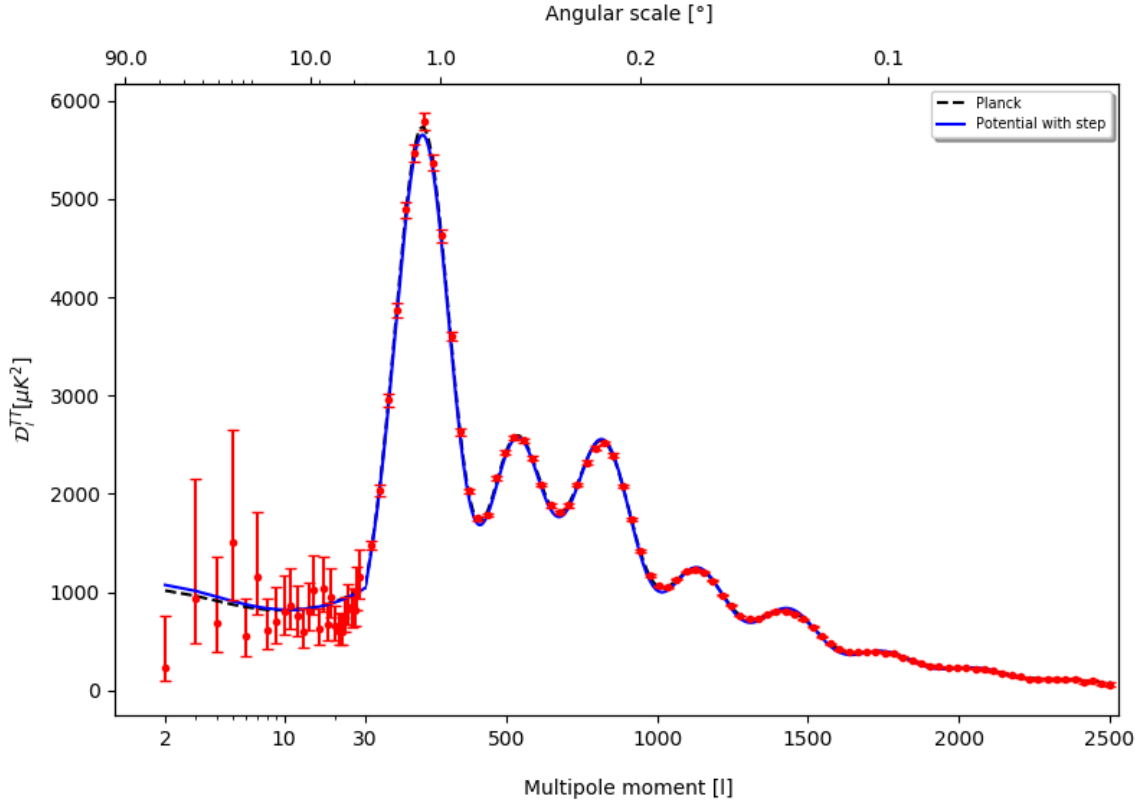
Figure 3.3: Best fit to Planck data for the chaotic potential with a step.

Comparing Fig. 3.2a and Fig. 3.2b, one can see that the uncertainty of the model is different for different regions of the power spectrum and the relative error goes from almost 0 to less than 0.09. These two figures show that our model at intermediate angular scales ($100 \lesssim l \lesssim 1000$) exhibits a low relative error (around 2%) and at large angular scales ($l \lesssim 100$) the relative error is larger (compared to intermediate angular scales, although it is still low, around 6%). Fig. 3.2b shows that the uncertainty is larger for small angular scales($l \gtrsim 1000$), although we can realize that it exhibits oscillations with respect to the Planck data. As a result, even if the uncertainty is larger with respect to the other two regions, there are points where the relative errors drops to almost zero.

From this quantitative analysis of the obtained temperature power spectrum, one can say that this model reproduce to a good level the temperature fluctuations present at the early universe. Besides, it reproduces pretty well the acoustic oscillations, since these are present at intermediate angular scales, this part of the spectrum has the smallest uncertainty ($\sim$ 2%). Finally, Fig. 3.3 shows the power spectrum obtained with the potential of Eq. (3.1) and with the parameters that display the lowest relative error, $c = 0.08$, $d = 0.03$ and $\phi_{\text{step}} = 14.09$.

3.2 Large angular scales

At large angular scales the contribution to the CMB anisotropies comes from perturbations that are superhorizon at recombination[51]. At these scales is present relatively unprocessed primordial fluctuation spectrum due to the distance of patches on the sky[18]. Large angular scales of the angular power spectrum is shown in Fig. 3.4.

Figure 3.4: Large angular scales region. The blue line was obtained with the chaotic potential with a step and the black dashed line is from Planck data.

At these scales the Sachs–Wolfe (SW) effect and Integrated Sachs–Wolfe (ISW) effect dominates for the shape of the spectrum[51]. The SW effect was pointed out by Sachs and Wolfe[11] in 1967 and it is the result of spatial fluctuations in the gravitational potential at the Last Scattering Surface (LSS) which causes a red and/or blue shifts in the frequency of photons[57]. In a high density region, compared to the average at LSS, photons are gravitationally redshifted when they try to escape from the potential well, varying their temperature. The ISW is produced by the variation over time of gravitational potentials, this have changed the temperature of the photons between decoupling and the present.

The ISW effect emerges at transient epochs and it can be divided in two. The early ISW emerges during the

transition from radiation dominated era to matter dominated era, while the late ISW emerges during the transition from matter dominated era to dark energy dominated era. Acording to Fig. 3.4 and Fig. 3.2b the difference of our model with respect to data is larger for small l. Late ISW effect is present at small $l \sim 2-4$. The measurement of the late ISW effect is associated with obtaining a information of dark energy[51], then the model may present some difference at predicting the amount of dark energy present in the universe. This will be discussed in the following section.

3.3   Intermediate angular scales

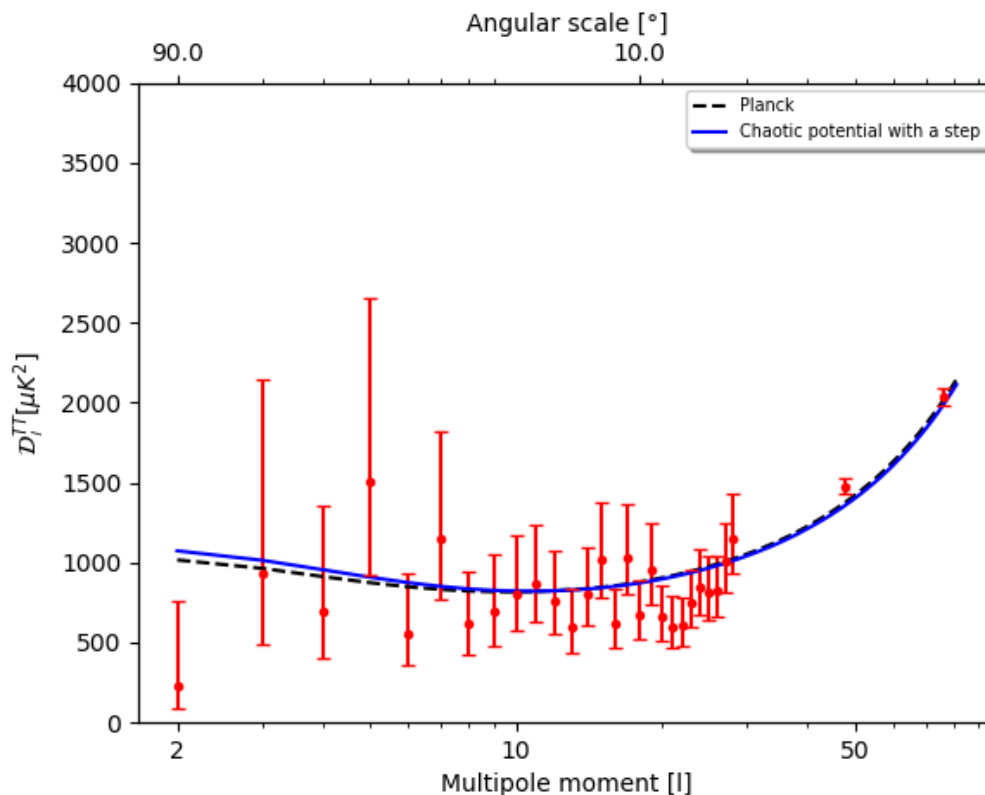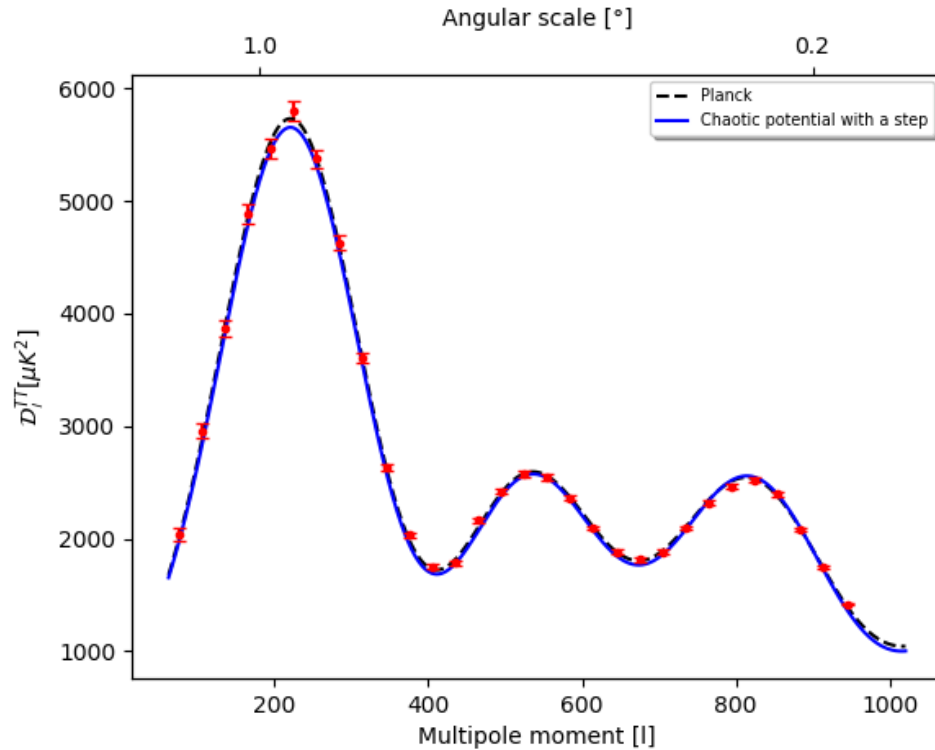Figure 3.5: Intermediate angular scales region. The blue line was obtained with the chaotic potential with a step and the black dashed line is from Planck data.

Before recombination photons and baryons were coupled through Compton and Coulomb interactions, this allows us to consider them as a mixed compressive fluid[58]. In a compressive fluid the density perturbations are just acoustic waves. As soon as a perturbation enters the sound horizon of the fluid, it starts to oscillate. Fig. 3.5 shows the the presence of acoustic oscillations at intermediate angular scales.

These oscillations are the result of an interplay of pressure and gravitational attraction. The gravitational attraction is created by overdensities in the fluid produced by dark matter that attracts baryons and photons, this generates a pressure on the fluid that opposes gravity and leads matter and photons away (rarefaction). As the pressure decreases, gravity takes over and compresses the fluid once again; this cycle produce the oscillations. The region of $100 \lesssim l \lesssim 1000$ is composed by tree peaks and two troughs as one can see in Fig. 3.5. The first peak in the angular power spectrum is the fundamental mode which was caught in its first compression, when it achieved its maximum density and temperature. The second peak is the mode that had time to perform a full cycle of compression and rarefaction before recombination took place[59]. The third peak correspond to a mode that had time to perform two complete collapses before recombination and so on with the following peaks at small angular scales. In Table 3.1 appear the peaks, with their position and amplitude reported by Planck Collaboration and the ones obtained using the chaotic potential with a step of Eq. (3.1).

Table 3.1: Peaks and troughs of the CMB angular power spectrum reported by Planck satellite and peaks obtained using the chaotic potential with a step.

Extremum	Multipole [l]	Amplitude [μK^2]
Planck results		
Peak 1	220.6 ± 0.6	5733 ± 39
Trough 1	416.3 ± 1.1	1713 ± 20
Peak 2	538.1 ± 1.3	2586 ± 23
Trough 2	675.5 ± 1.2	1799 ± 14
Peak 3	809.8 ± 1.0	2518 ± 17
Chaotic potential with a step		
Peak 1	221	5652.65
Trough 1	411	1683.98
Peak 2	537	2573.24
Trough 2	674	1765.82
Peak 3	814	2556.88

Cosmological parameters are directly related with the peak characteristics of the angular power spectrum[18,60] ; position (l) and amplitud (μK^2). Table 3.2 shows some cosmological parameters reported by Planck and the values obtained using the chaotic potential with a step. The position of the first peak has a strong relation with the age of the Universe[60]. From Table 3.1 we find that the Planck results give the position of the first peak at 220.6 ± 0.6, while our model gives $l = 221$ for the position of the first peak. It is inside the range, therefore there could be a small difference in the age of the Universe reported by Planck Collaboration and the age predicted by our model. Looking at Table 3.2 one find that the age reported by Planck is 13.797 ± 0.023 Gyrs and the one we predicted is 13.798 Gyrs which has a difference of the order of 10^{-3}, but still inside the range of the error.

The value of the first peak is also directly related to Ω_m, since decreasing the height of the first peak increases

Table 3.2: Cosmic parameters reported by Planck and the ones obtained for the chaotic potential with a step.

Parameter	Planck	Step potential
Age(Gyrs)	13.797 ± 0.023	13.798
Ω_m	0.3153 ± 0.0073	0.315823
$\Omega_b h^2$	0.02237 ± 0.00015	0.022383
Ω_Λ	0.6847 ± 0.0073	0.684097
Ω_K	-0.0096 ± 0.0061	0.00000
n_s	0.9649 ± 0.0042	0.966942

Ω_m. This happens because the the depth of the well is decreased due to the additional mass loading of the fluid [18]. In Fig. 3.5 we can see that the angular power spectrum obtained with our model is lower in the first peak. Besides, in Table 3.2 amplitude reported by Planck is $5733 \pm 39\,\mu K^2$ and our model gives $5652.65\,\mu K^2$. These difference is reflected in the difference of Ω_m shown in Table 3.2. Our model gives $\Omega_m = 0.315823$ and the value reported by Planck is $\Omega_m = 0.3153 \pm 0.0073$. As one could expect, the value obtained from our model is larger, since the height of the first peak is lower.

The most important feature of the second peak is that increasing Ω_b decreases its height. This happens beacuse as one increases Ω_b, it also increases the inertia in the photon-baryon fluid [18] which results in a smaller rarefaction and a lower peak. In Table 3.1 peak 2 reported by Planck Collaboration has an amplitude of $2586 \pm 23\,\mu K^2$ while the value obtained by our model is $2573.24\,\mu K^2$. Table 3.2 shows that Planck reported $\Omega_b h^2 = 0.02237 \pm 0.00015$ while our model gives $\Omega_b h^2 = 0.022383$, the difference is small but the statement holds. On the other hand, for the third peak increasing Ω_b increases its height and increasing Ω_m decreases its height. The third peak has an amplitude of $518 \pm 17\,\mu K^2$ reported by Planck and the value obtained for our model is $2556.88\,\mu K^2$.

The position of the peaks are also sensitive to the spatial curvature and at a lower level to the dark matter and dark energy densities [51]. As we saw, the positions of the first and second peak obtained with our model are similar to the ones reported by Planck. However, the position of the third peak gives a larger difference, Planck reported the third peak at $l = 809.8 \pm 1.0$ while in our model it is at $l = 814$. From Table 3.2 the values reported by Planck are $\Omega_\Lambda = 0.6847 \pm 0.0073$ and $\Omega_K = -0.0096 \pm 0.0061$, while our model gives $\Omega_\Lambda = 0.684097$ and $\Omega_K = 0.0$ which would explain the different position of the third peak.

The second peak also depends on n_s and is the result of the overall slope of the CMB angular power spectrum. The relation is: increasing n_s increases the height of the second peak relative to the first. Planck reported $n_s = 0.9649 \pm 0.0042$ and our model gives a larger value $n_s = 0.966942$. Computing the height of the second peak relative to the first peak for the Planck data gives 0.4528 while for our model gives 0.4552 which confirms the previous statement.

3.4 Small angular scales

At small angular scales there are two important effects that occurs at recombination. The first effect is known as Silk damping which is the responsible for the suppression of acoustic oscillations in baryon-photon fluid[51]. During the process of recombination the mean free path of photons is large and number density of electrons is small. Here, photons from overdense regions travel large distances and tranfer their energy to underdense regions, this erases the density fluctuations. The other effect is produced because photons do not decouple simultaneously, which leads to the suppression of the angular spectrum at small angular scales[51].
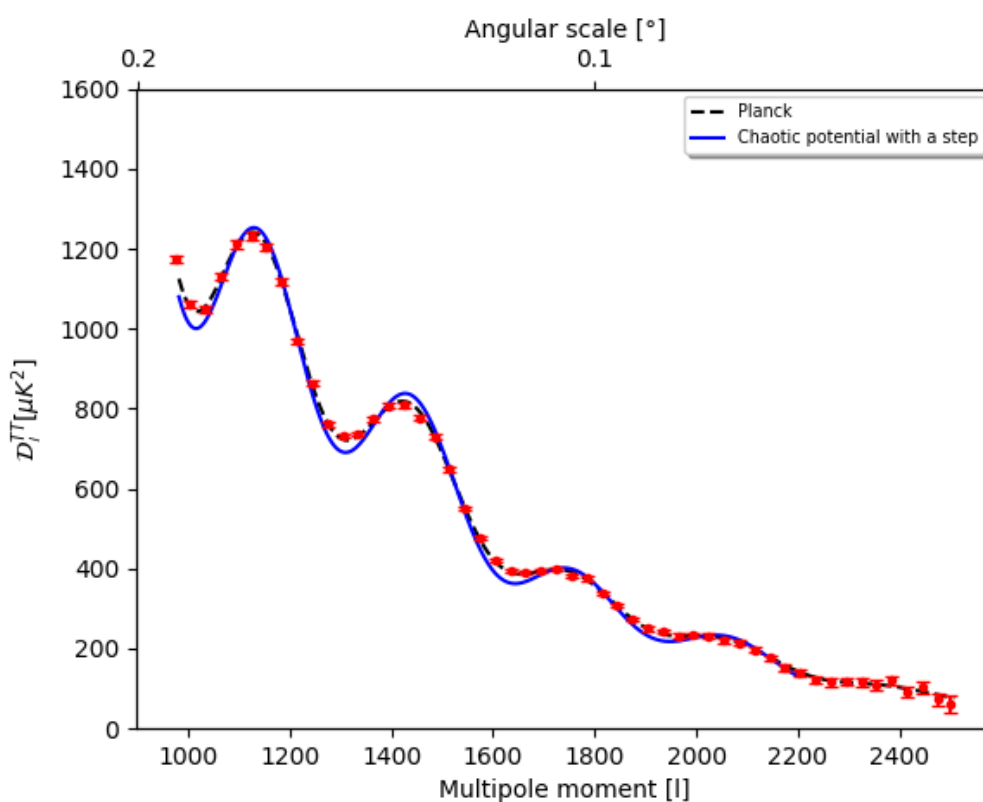
Figure 3.6: Small angular scales region. The blue line was obtained with the chaotic potential with a step and the black dashed line is from Planck data.

The shape of the damping tail is related to Ω_b, since increasing Ω_b increases the coupling of the photon-baryon fluid. This produce that the damping tail shifts to smaller angular scales because the mean free path of the photons has been reduced. Since the value of Ω_b predicted by our model is larger (by a small amount), we expect to see in Fig. 3.6 a small shift to the right (to smaller angular scales).

Fig. 3.2b shows that at these scales the percentage error of our model is larger than percentage error of large

and intermediate scales. Comparing with Fig. 3.2a one can appreciate that the peaks present lower error than the troughs and Fig. 3.6 seems to corroborate this.

3.5   Methodology

The results shown in this chapter were obtained by using Mathematica to get the tensor and scalar spectral indices and their respective runing terms, different values for ϕ_{step}, c and d were used. This was made numerically due to the nature of the equations that do not let compute analytically some results, as it will be shown. After getting these values, it was used the CAMB code to obtain different scalar power spectra.

Recall that for a single field model, the slow roll parameters are

$$\epsilon_V = \frac{M^2}{2} \left(\frac{V'}{V} \right)^2 , \qquad \eta_V = M^2 \left(\frac{V''}{V} \right), \tag{3.2}$$

and

$$\xi_v^2 = \frac{M^4 V'(\phi) V'''(\phi)}{V^2(\phi)}, \qquad \varpi_v^3 = \frac{M^6 V'^2(\phi) V''''(\phi)}{V^3(\phi)}. \tag{3.3}$$

The number of e-folds is defined as

$$N = \int_t^{t_{end}} H \, dt \simeq \frac{1}{M_{pl}^2} \int_{\phi_f}^{\phi_i} \frac{V}{V'} d\phi = \int_{\phi_f}^{\phi_i} \frac{1}{\sqrt{2\epsilon_V}} \frac{d\phi}{M_{pl}}. \tag{3.4}$$

Using these definitions and some others of chapter 2, we look for the values we need to use in CAMB code.

3.5.1   "Chaotic potential"

The "chaotic potential" is

$$V(\phi) = \frac{1}{2} m^2 \phi^2, \tag{3.5}$$

from which the slow roll parameters are

$$\epsilon_V = 2 \frac{M_{pl}^2}{\phi^2}, \quad \eta_V = 2 \frac{M_{pl}^2}{\phi^2}, \quad \xi_v^2 = 0, \quad \varpi_v^3 = 0. \tag{3.6}$$

Now, from Eq. 3.4, ϕ_i and ϕ_f are the values of the inflaton at the beginning and at the end of inflation, respectively. Since $\epsilon_V = 1$ at the end of inflation, we can compute ϕ_f and one gets

$$\phi_f = \sqrt{2} M_{pl} \tag{3.7}$$

and the value of the inflaton in terms of N is

$$\phi = 2 M_{pl} \sqrt{N + \frac{1}{2}} \approx 2 M_{pl} \sqrt{N}. \tag{3.8}$$

Then, the analytic prediction for the inflationary parameters in terms of N are

$$n_s = 1 - \frac{2}{N}, \tag{3.9}$$

$$n_t = -\frac{1}{N}, \tag{3.10}$$

$$\frac{dn_s}{d\ln k} = -\frac{2}{N^2}, \tag{3.11}$$

$$\frac{dn_t}{d\ln k} = \frac{1}{N^2}, \tag{3.12}$$

$$\frac{d^2 n_s}{d\ln k^2} = -\frac{7}{N^3}, \tag{3.13}$$

$$r = \frac{8}{N}. \tag{3.14}$$

3.5.2 Chaotic potential with a step

The model used for this work is a chaotic potential with a step of Eq. (3.1), for this potential the slow roll parameters are

$$\epsilon_V = \frac{\left\{ 2d \left[1 + c\tanh\left(\frac{\phi - \phi_{\text{step}}}{d}\right) \right] + c\phi \operatorname{sech}^2\left(\frac{\phi - \phi_{\text{step}}}{d}\right) \right\}^2}{2d^2 \phi^2 \left[1 + c\tanh\left(\frac{\phi - \phi_{\text{step}}}{d}\right) \right]^2}, \tag{3.15}$$

$$\eta_V = \frac{2 \left\{ d^2 \left[1 + c\tanh\left(\frac{\phi - \phi_{\text{step}}}{d}\right) \right] + c\phi \operatorname{sech}^2\left(\frac{\phi - \phi_{\text{step}}}{d}\right) \left[2d - \phi\tanh\left(\frac{\phi - \phi_{\text{step}}}{d}\right) \right] \right\}}{d^2 \phi^2 \left[1 + c\tanh\left(\frac{\phi - \phi_{\text{step}}}{d}\right) \right]}, \tag{3.16}$$

$$
\begin{aligned}
\xi_v^2 = {} & \frac{1}{d^4 \phi^3 \left[1 + c\tanh\left(\frac{\phi - \phi_{\text{step}}}{d}\right) \right]^2} c\operatorname{sech}^4\left(\frac{\phi - \phi_{\text{step}}}{d}\right) \\
& \times \left[3d^2 - 4\phi^2 + (3d^2 + 2\phi^2)\cosh\left(\frac{2(\phi - \phi_{\text{step}})}{d}\right) - 6d\phi\sinh\left(\frac{2(\phi - \phi_{\text{step}})}{d}\right) \right] \\
& \times \left\{ 2d \left[1 + c\tanh\left(\frac{\phi - \phi_{\text{step}}}{d}\right) \right] + c\phi\operatorname{sech}^2\left(\frac{\phi - \phi_{\text{step}}}{d}\right) \right\},
\end{aligned}
\tag{3.17}
$$

$$
\begin{aligned}
\varpi_V^3 = {} & -\frac{1}{d^5 m^2 \phi^5 \left[1 + c\tanh\left(\frac{\phi - \phi_{\text{step}}}{d}\right) \right]^3} 16c\operatorname{sech}^2\left(\frac{\phi - \phi_{\text{step}}}{d}\right) \left[d - \phi\tanh\left(\frac{\phi - \phi_{\text{step}}}{d}\right) \right] \\
& \times \left[-\phi + 3\phi\operatorname{sech}^2\left(\frac{\phi - \phi_{\text{step}}}{d}\right) + 3d\tanh\left(\frac{\phi - \phi_{\text{step}}}{d}\right) \right] \\
& \times \left\{ 2d \left[1 + c\tanh\left(\frac{\phi - \phi_{\text{step}}}{d}\right) \right] + c\phi\operatorname{sech}^2\left(\frac{\phi - \phi_{\text{step}}}{d}\right) \right\}.
\end{aligned}
\tag{3.18}
$$

Unlike the simple chaotic potential, in this case there is no analytical solution for ϕ. Therefore, the software Wolfram Mathematica was used to obtain the values for the tensor and scalar spectral indices and their corresponding running terms. The values obtained with our model show smaller values for the running terms of the scalar spectral index, however, it is consistent with a vanishing running of the scalar spectral index.

Table 3.3: Values of the scalar index and their running terms reported by Planck Collaboration and the values obtained for the chaotic potential with a step.

Definition	Parameter	Planck	Step potential
Scalar spectral index	n_s	0.9649 ± 0.0042	0.966942
Running of scalar spectral index	$dn_s/d\ln k$	-0.0045 ± 0.0067	-0.000546404
Running of running of scalar spectral index	$d^2 n_s/d\ln k^2$	0.022 ± 0.012	-0.0000180628
Tensor-to-scalar ratio	r	<0.1	0.132231

Chapter 4

Conclusions & Outlook

This thesis aimed to study the angular power spectrum of the CMB with the chaotic inflationary model with a step. For this purpose, the software Wolfram Mathematica and Code for Anisotropies in the Microwave Background (CAMB) were used. The former helped to obtain spectral indices and running terms needed to work with CAMB. The second one allows to obtain the value the shape of the angular power spectrum and the value of the cosmological parameters for our model.

Our potential have three free parameters which were adjusted to obtain the closest shape to the temperature power spectrum reported by Planck Collaboration[23]. The values that allows to have the best fit are: $c = 0.08$, $d = 0.03$ and $\phi_{step} = 14.09$. Fig. 3.2 shows that the choice of this parameters gives a relative error below 0.09 or a percentage error $< 9\%$. The following step was to separate the power spectrum in three parts and analyze each one. The first part corresponds to a large angular scales ($l \lesssim 100$), the second part corresponds to intermediate angular scales ($100 \lesssim l \lesssim 1000$) and the third part corresponds to small angular scales ($l \gtrsim 1000$).

For large scales, our model shows a larger differences at small $l \sim 2 - 4$. Since at these scales the late Integrated Sachs–Wolfe (ISW) is present, the value we obtain for Ω_Λ is different from the value reported by Plank as shown in Table 3.2. The part of the spectrum that shows the smallest difference is the region of intermediate angular scales.

At intermediate angular scales our model shows a small deviation from the shape of the power spectrum obtained using Planck data, the relative error is ~ 0.02. Since the oscillations present in the power spectrum are related with the dynamics of the baryon-photon fluid present before recombination, we could expect small differences for Ω_m and Ω_b compared to Planck data. In Table 3.2 corroborates that the values of Ω_m and Ω_b obtained with our model are inside the range of the error reported by Planck. Additionally, the position (l) of the first peak is related to the age of the Universe and the value obtained with our model ($l = 221$) is close to the value reported by Planck ($l = 220.6 \pm 0.6$). Table 3.2 shows that the age of the universe obtained for our model is close to the value reported by Planck.

At large angular scales the difference between Planck data and our model is larger compared to the other regions. Besides, our spectrum exhibits a small shit to the right due to the small difference in Ω_b. The position of the peaks are sensitive to the spatial curvature and the dark matter and dark energy densities, which explains the difference in

the position of the third peak (Table 3.1) and the shift of the tail of the spectrum.

The value of the n_s is larger for our model, which is expected since the height of the second peak relative to the first peak is larger. The values of the running terms are lower than the ones reported by Planck, nevertheless, this is consistent with a vanishing running of the scalar spectral index.

Finally, future works could consider other potentials with a step to evaluate the possibility of model the angular power spectrum of the Cosmic Microwave Background (CMB) with a higher accuracy. Another option is to consider models with concave potentials since these are consistent with Planck data.

Bibliography

[1] Freedman, W. L.; Madore, B. F.; Gibson, B. K.; Ferrarese, L.; Kelson, D. D.; Sakai, S.; Mould, J. R.; Kennicutt Jr, R. C.; Ford, H. C.; Graham, J. A. Final results from the Hubble Space Telescope key project to measure the Hubble constant. *The Astrophysical Journal* **2001**, *553*, 47.

[2] Steigman, G. Primordial nucleosynthesis in the precision cosmology era. *Annu. Rev. Nucl. Part. Sci.* **2007**, *57*, 463–491.

[3] Pospelov, M.; Pradler, J. Big bang nucleosynthesis as a probe of new physics. *Annual Review of Nuclear and Particle Science* **2010**, *60*, 539–568.

[4] Fixsen, D.; Cheng, E.; Gales, J.; Mather, J. C.; Shafer, R.; Wright, E. The cosmic microwave background spectrum from the full cobe* firas data set. *The Astrophysical Journal* **1996**, *473*, 576.

[5] Dodelson, S.; Schmidt, F. *Modern cosmology*; Academic Press, 2020.

[6] Reichardt, C.; Ade, P. A.; Bock, J.; Bond, J. R.; Brevik, J.; Contaldi, C.; Daub, M.; Dempsey, J.; Goldstein, J.; Holzapfel, W.; et al., High-resolution CMB power spectrum from the complete ACBAR data set. *The Astrophysical Journal* **2009**, *694*, 1200.

[7] Alpher, R. A.; Herman, R. Evolution of the Universe. *Nature* **1948**, *162*, 774–775.

[8] Penzias, A. A.; Wilson, R. W. A measurement of excess antenna temperature at 4080 Mc/s. *The Astrophysical Journal* **1965**, *142*, 419–421.

[9] Fixsen, D. The temperature of the cosmic microwave background. *The Astrophysical Journal* **2009**, *707*, 916.

[10] Durrer, R. The cosmic microwave background: the history of its experimental investigation and its significance for cosmology. *Classical and Quantum Gravity* **2015**, *32*, 124007.

[11] Sachs, R. K.; Wolfe, A. M. Perturbations of a cosmological model and angular variations of the microwave background. *The Astrophysical Journal* **1967**, *147*, 73.

[12] Silk, J. Cosmic black-body radiation and galaxy formation. *The Astrophysical Journal* **1968**, *151*, 459.

[13] Peebles, P. J.; Yu, J. Primeval adiabatic perturbation in an expanding universe. *The Astrophysical Journal* **1970**, *162*, 815.

[14] Sunyaev, R.; Zel'Dovich, Y. B. Microwave background radiation as a probe of the contemporary structure and history of the universe. *Annual review of astronomy and astrophysics* **1980**, *18*, 537–560.

[15] Cheng, E.; Saulson, P.; Wilkinson, D.; Corey, B. Large-scale anisotropy in the 2.7 K radiation. *The Astrophysical Journal* **1979**, *232*, L139–L143.

[16] Smoot, G. F.; Gorenstein, M. V.; Muller, R. A. Detection of anisotropy in the cosmic blackbody radiation. *Physical Review Letters* **1977**, *39*, 898.

[17] Smoot, G. F.; Bennett, C. L.; Kogut, A.; Wright, E.; Aymon, J.; Boggess, N.; Cheng, E.; De Amici, G.; Gulkis, S.; Hauser, M. Structure in the COBE differential microwave radiometer first-year maps. *The Astrophysical Journal* **1992**, *396*, L1–L5.

[18] Page, L.; Hinshaw, G.; Kogut, A.; Spergel, D.; Tucker, G.; Jarosik, N.; Halpern, M.; Limon, M.; Bennett, C.; Meyer, S. First Year Wilkinson Microwave Anisotropy Probe (WMAP) Observations: Preliminary Maps and Basic Results. **2003**,

[19] Spergel, D. N.; Verde, L.; Peiris, H. V.; Komatsu, E.; Nolta, M.; Bennett, C. L.; Halpern, M.; Hinshaw, G.; Jarosik, N.; Kogut, A. First-year Wilkinson Microwave Anisotropy Probe (WMAP)* observations: determination of cosmological parameters. *The Astrophysical Journal Supplement Series* **2003**, *148*, 175.

[20] Bennett, C. L.; Larson, D.; Weiland, J. L.; Jarosik, N.; Hinshaw, G.; Odegard, N.; Smith, K.; Hill, R.; Gold, B.; Halpern, M. Nine-year Wilkinson Microwave Anisotropy Probe (WMAP) observations: final maps and results. *The Astrophysical Journal Supplement Series* **2013**, *208*, 20.

[21] Ade, P. A.; Aghanim, N.; Arnaud, M.; Ashdown, M.; Aumont, J.; Baccigalupi, C.; Banday, A.; Barreiro, R.; Bartlett, J.; Bartolo, N. Planck 2015 results-xiii. cosmological parameters. *Astronomy & Astrophysics* **2016**, *594*, A13.

[22] Akrami, Y.; Arroja, F.; Ashdown, M.; Aumont, J.; Baccigalupi, C.; Ballardini, M.; Banday, A. J.; Barreiro, R.; Bartolo, N.; Basak, S.; et al, Planck 2018 results-X. Constraints on inflation. *Astronomy & Astrophysics* **2020**, *641*, A10.

[23] Aghanim, N.; Akrami, Y.; Arroja, F.; Ashdown, M.; Aumont, J.; Baccigalupi, C.; Ballardini, M.; Banday, A. J.; Barreiro, R.; Bartolo, N.; et al, Planck 2018 results-I. Overview and the cosmological legacy of Planck. *Astronomy & Astrophysics* **2020**, *641*, A1.

[24] Guth, A. H. Inflation and eternal inflation. *Physics Reports* **2000**, *333*, 555–574.

[25] Preskill, J. P. Cosmological production of superheavy magnetic monopoles. *Physical Review Letters* **1979**, *43*, 1365.

[26] Harrison, E. R. Fluctuations at the threshold of classical cosmology. *Physical review D* **1970**, *1*, 2726.

[27] Liddle, A. *An introduction to modern cosmology; 2nd ed.*; Wiley: Chichester, 2003.

[28] Frieman, J. A.; Turner, M. S.; Huterer, D. Dark energy and the accelerating universe. *Annu. Rev. Astron. Astrophys.* **2008**, *46*, 385–432.

[29] Friedmann, A. Über die krümmung des raumes. *Zeitschrift fur Physik* **1922**, *10*, 377–386.

[30] Lemaître, G. Un Univers homogène de masse constante et de rayon croissant rendant compte de la vitesse radiale des nébuleuses extra-galactiques. 1927.

[31] Hubble, E. P. 106. A Relation between Distance and Radial Velocity among Extra-Galactic Nebulae. *Proceedings of the National Academy of Sciences* **1929**, 168–173.

[32] Riess, A. G.; Macri, L. M.; Hoffmann, S. L.; Scolnic, D.; Casertano, S.; Filippenko, A. V.; Tucker, B. E.; Reid, M. J.; Jones, D. O.; Silverman, J. M. A 2.4% determination of the local value of the Hubble constant. *The Astrophysical Journal* **2016**, *826*, 56.

[33] Hinshaw, G.; Larson, D.; Komatsu, E.; Spergel, D. N.; Bennett, C.; Dunkley, J.; Nolta, M.; Halpern, M.; Hill, R.; Odegard, N. Nine-year Wilkinson Microwave Anisotropy Probe (WMAP) observations: cosmological parameter results. *The Astrophysical Journal Supplement Series* **2013**, *208*, 19.

[34] Reid, M.; Braatz, J.; Condon, J.; Lo, K.; Kuo, C.; Impellizzeri, C.; Henkel, C. The megamaser cosmology project. IV. A direct measurement of the Hubble constant from UGC 3789. *The Astrophysical Journal* **2013**, *767*, 154.

[35] Kuo, C.; Braatz, J.; Lo, K.; Reid, M.; Suyu, S.; Pesce, D.; Condon, J.; Henkel, C.; Impellizzeri, C. The megamaser cosmology project. VI. Observations of NGC 6323. *The Astrophysical Journal* **2015**, *800*, 26.

[36] Gao, F.; Braatz, J.; Reid, M.; Lo, K.; Condon, J.; Henkel, C.; Kuo, C.; Impellizzeri, C.; Pesce, D.; Zhao, W. The megamaser cosmology project. VIII. A geometric distance to NGC 5765b. *The Astrophysical Journal* **2016**, *817*, 128.

[37] Suyu, S.; Auger, M.; Hilbert, S.; Marshall, P.; Tewes, M.; Treu, T.; Fassnacht, C.; Koopmans, L.; Sluse, D.; Blandford, R. Two accurate time-delay distances from strong lensing: Implications for cosmology. *The Astrophysical Journal* **2013**, *766*, 70.

[38] Suyu, S. H.; Treu, T.; Hilbert, S.; Sonnenfeld, A.; Auger, M. W.; Blandford, R. D.; Collett, T.; Courbin, F.; Fassnacht, C. D.; Koopmans, L. V. Cosmology from gravitational lens time delays and Planck data. *The Astrophysical Journal Letters* **2014**, *788*, L35.

[39] Wong, K. C.; Suyu, S. H.; Auger, M. W.; Bonvin, V.; Courbin, F.; Fassnacht, C. D.; Halkola, A.; Rusu, C. E.; Sluse, D.; Sonnenfeld, A. H0LiCOW–IV. Lens mass model of HE 0435- 1223 and blind measurement of its time-delay distance for cosmology. *Monthly Notices of the Royal Astronomical Society* **2017**, *465*, 4895–4913.

[40] Abbott, B.; Abbott, R.; Abbott, T.; Abraham, S.; Acernese, F.; Ackley, K.; Adams, C.; Adhikari, R.; Adya, V.; Affeldt, C.; et al, A gravitational-wave measurement of the Hubble constant following the second observing run of Advanced LIGO and Virgo. *The Astrophysical Journal* **2021**, *909*, 218.

[41] Guidorzi, C.; Margutti, R.; Brout, D.; Scolnic, D.; Fong, W.; Alexander, K.; Cowperthwaite, P.; Annis, J.; Berger, E.; Blanchard, P. Improved constraints on H 0 from a combined analysis of gravitational-wave and electromagnetic emission from GW170817. *The Astrophysical Journal Letters* **2017**, *851*, L36.

[42] Schramm, D. N.; Turner, M. S. Big-bang nucleosynthesis enters the precision era. *Reviews of Modern Physics* **1998**, *70*, 303.

[43] Iocco, F.; Mangano, G.; Miele, G.; Pisanti, O.; Serpico, P. D. Primordial Nucleosynthesis: from precision cosmology to fundamental physics. *Physics Reports* **2009**, *472*, 1–76.

[44] Olive, K. A. Big bang nucleosynthesis. *Nuclear Physics B-Proceedings Supplements* **2000**, *80*, 79–93.

[45] Bennett, C. L.; Banday, A. J.; Górski, K. M.; Hinshaw, G.; Jackson, P.; Keegstra, P.; Kogut, A.; Smoot, G. F.; Wilkinson, D. T.; Wright, E. L. Four-year COBE* DMR cosmic microwave background observations: maps and basic results. *The Astrophysical Journal Letters* **1996**, *464*, L1.

[46] Komatsu, E.; Smith, K. M.; Dunkley, J.; Bennett, C. L.; Gold, B.; Hinshaw, G.; Jarosik, N.; Larson, D.; Nolta, M. R.; Page, L.; et al., SEVEN-YEAR WILKINSON MICROWAVE ANISOTROPY PROBE (WMAP) OBSERVATIONS: COSMOLOGICAL INTERPRETATION. *The Astrophysical Journal Supplement Series* **2011**, *192*, 18.

[47] Senatore, L. Lectures on inflation. *Theoretical Advanced Study Institute in Elementary Particle Physics: new frontiers in fields and strings* **2016**, 447–543.

[48] Clesse, S. An introduction to inflation after Planck: from theory to observations. *arXiv preprint arXiv:1501.00460* **2015**,

[49] Senatore, L. TASI 2012 lectures on inflation. *Theoretical Advanced Study Institute in Elementary Particle Physics: Searching for New Physics at Small and Large Scales* **2013**, 221–302.

[50] Tojeiro, R. Understanding the Cosmic Microwave Background temperature power spectrum. *alm* **2006**, *2*, 6.

[51] Gorbunov, D. S.; Rubakov, V. A. *Introduction to the theory of the early universe: Cosmological perturbations and inflationary theory*; World Scientific, 2011.

[52] Linde, A. D. Chaotic inflation. *Physics Letters B* **1983**, *129*, 177–181.

[53] Lewis, A. `https://cosmologist.info/notes/CAMB.pdf`.

[54] Lewis, A.; Bridle, S. Cosmological parameters from CMB and other data: A Monte Carlo approach. *Physical Review D* **2002**, *66*, 103511.

[55] Howlett, C.; Lewis, A.; Hall, A.; Challinor, A. CMB power spectrum parameter degeneracies in the era of precision cosmology. *Journal of Cosmology and Astroparticle Physics* **2012**, *2012*, 027.

[56] Challinor, A.; Lewis, A. Linear power spectrum of observed source number counts. *Physical Review D* **2011**, *84*, 043516.

[57] Casas, S. Power Spectrum and the Anisotropies of the CMB.

[58] Sugiyama, N. Introduction to temperature anisotropies of Cosmic Microwave Background radiation. *Progress of Theoretical and Experimental Physics* **2014**, *2014*, 06B101.

[59] Hu, W.; Dodelson, S. Cosmic microwave background anisotropies. *Annual Review of Astronomy and Astrophysics* **2002**, *40*, 171–216.

[60] Hu, W.; Fukugita, M.; Zaldarriaga, M.; Tegmark, M. Cosmic microwave background observables and their cosmological implications. *The Astrophysical Journal* **2001**, *549*, 669.

Abbreviations

BBN Big Bang Nucleosynthesis ix, 6–9, 13

CAMB Code for Anisotropies in the Microwave Background iii, 2, 21, 23, 32, 35
CMB Cosmic Microwave Background iii, ix, 1–4, 9–11, 13, 17, 21, 23, 30, 36
COBE Cosmic Background Explorer 1, 24

FIRAS Far-InfraRed Absolute Spectrophotometer 1, 10
FRW Friedmann–Robertson–Walker 3, 4, 10, 15

GR General Relativity 3, 4

ISW Integrated Sachs–Wolfe 27, 28, 35

LSS Last Scattering Surface ix, 9, 11, 27

SW Sachs–Wolfe 27

WMAP Wilkinson Microwave Anisotropy Probe 2, 24